Li *et al. Microbiome* (2024) 12:202
https://doi.org/10.1186/s40168-024-01928-4

Microbiome

RESEARCH

Open Access

An iron-binding protein of entomopathogenic fungus suppresses the proliferation of host symbiotic bacteria

Juan Li[1,2], Jiujie Li[1,2], Lili Cao[1], Qinghua Chen[1,2], Ding Ding[1*] and Le Kang[1,2*]

Abstract

Background Entomopathogenic fungal infection-induced dysbiosis of host microbiota offers a window into understanding the complex interactions between pathogenic fungi and host symbionts. Such insights are critical for enhancing the efficacy of mycoinsecticides. However, the utilization of these interactions in pest control remains largely unexplored.

Results Here, we found that infection by the host-specialist fungus *Metarhizium acridum* alters the composition of the symbiotic microbiota and increases the dominance of some bacterial symbionts in locusts. Meanwhile, *M. acridum* also effectively limits the overgrowth of the predominant bacteria. Comparative transcriptomic screening revealed that the fungus upregulates the production of MaCFEM1, an iron-binding protein, in the presence of bacteria. This protein sequesters iron, thereby limiting its availability. Functionally, overexpression of MaCFEM1 in the fungus induces iron deprivation, which significantly suppresses bacterial growth. Conversely, *MaCFEM1* knockout relieves the restriction on bacterial iron availability, resulting in iron reallocation. Upon Δ*MaCFEM1* infection, some host bacterial symbionts proliferate uncontrollably, turning into opportunistic pathogens and significantly accelerating host death.

Conclusions This study elucidates the critical role of pathogenic fungal-dominated iron allocation in mediating the shift of host microbes from symbiosis to pathogenicity. It also highlights a unique biocontrol strategy that jointly exploits pathogenic fungi and bacterial symbionts to increase host mortality.

Introduction

Successful pathogens are capable of modifying the internal environment of their hosts and take advantage of the host microbiota to enhance their within-host fitness [1, 2]. Conversely, the host microbiota typically serves as a barrier against the invasion of pathogens. However, there are instances in which some symbiotic microbes may inadvertently facilitate the pathogenic impact of invaders or even transform into pathogens themselves [3–5]. Thus, microbial interactions have profound effects on host health and can shape the evolution of host-microbe relationships. The elucidation of ecological effects and molecular mechanisms underlying the interactions

*Correspondence:
Ding Ding
dingding@ioz.ac.cn
Le Kang
lkang@ioz.ac.cn
[1] State Key Laboratory of Integrated Management of Pest Insects and Rodents, Institute of Zoology, Chinese Academy of Sciences, Beijing, China
[2] University of Chinese Academy of Sciences, Beijing, China

among hosts, symbiotic microbiota, and invading pathogens is crucial for the development of medicine and biocontrol technology.

Entomopathogenic fungi have been widely used in various agricultural pest controls and play a pivotal role in ecosystems by occupying diverse ecological niches [6–8]. These fungi initiate infection in insect hosts by piercing the exoskeleton with germinating spores and subsequently transforming into hyphal bodies within the hemocoel to assimilate nutrients for proliferation [9–11]. The host immune response is triggered when fungi adhere to and penetrate the cuticle. Additionally, bacteria present on the cuticle interact with the fungi during this process [12]. Therefore, during host infection, fungi face not only the host's immune system but also competition and potential antagonism from the host's symbiotic microbiota. Therefore, during host infection, fungi face not only the host's immune system but also competition and antagonism from the host's symbiotic microbiota. The bacteria residing on the epicuticle of many insects can inhibit the colonization of pathogenic fungi directly or indirectly through the production of multiple defense secretions [13, 14]. As an extension of cuticle inside insects, gut harbors a more diverse microbiome than epicuticle does. The conidia of a *M. anisopliae* only germinated in the gut of axenic desert locusts (*Schistocerca gregaria*), implying the potential antifungal role of gut microbiota [15]. Then, the gut microbial-derived compounds with antifungal activity have been isolated from a variety of insects [16–18]. During the infection, the host's hemocoel emerges as the principal niche for fungal entrenchment and expansion. This environment is characteristically deficient in symbiotic bacteria or presents them at an extremely low level. However, the invasion of entomopathogenic fungus can disrupt the composition of host microbiota, leading to the translocation and proliferation of symbiotic bacteria within the hemocoel [4, 19, 20]. The proliferation of the predominant symbiotic bacteria competes for nutritional resources with the fungus and potentially affects host survival. Recent studies suggest that *Beauveria* and *Metarhizium* species secrete antimicrobial peptides or secondary metabolites on the cuticle to inhibit the growth of Gram-positive bacteria and indirectly suppress the proliferation of predominant symbiotic bacteria in the hemocoel by affecting the host's immune responses [21–23], while the interrelationships between entomopathogenic fungi and symbiotic bacteria within host hemocoel are intricate and more than just the antagonism. A comprehensive understanding of the interactions between these microorganisms and the underlying molecular mechanisms can offer critical insights into enhancing the efficiency of biological control. However, purposeful manipulation of this process within a living system, based on the interplay among pathogenic fungi, symbionts, and the host, has not yet been explored.

While entomopathogenic fungi are considered an eco-friendly alternative to chemical pesticides, promoting their insecticidal efficacy remains a great challenge [24]. One effective strategy to augment the pathogenicity of these fungi is through genetic modification, such as the introduction of exogenous toxins or non-coding RNAs [25–27]. However, the use of transgenic fungal strains with exogenous genes or toxins may raise ecological safety concerns. Alternatively, since the proliferation of some symbiotic bacteria during fungal infection contributes to the host death [4], leveraging symbiotic microbes could offer another strategy for improving biocontrol technologies. By gaining a comprehensive understanding of the mechanisms underpinning fungal-bacterial interactions in the host and actively modulating these interactions, we have the potential to develop a unique and powerful approach to enhance the effectiveness of fungal biopesticides.

Locusts, with their swarming behavior and long-distance migration, are highly destructive pests globally [28–31]. Efforts to utilize entomopathogenic fungi, particularly the *Metarhizium* spp., for locust plague control have been in practice since the 1990s [32]. *M. acridum*, a host-specialist that only infects grasshoppers and locusts [33], exhibits greater lethality against these hosts compared to some host-generalist *Metarhizium* species [34, 35]. Considering the approximately 48 million years of coevolution between *M. acridum* and locusts, this host–pathogen system may offer a well-developed model for studying the within-host microbial interactions [36, 37]. The present study reveals that suppression of the fungal iron-binding protein's expression can prompt a shift of commensal bacteria into opportunistic pathogens, which consequently shortens the lifespan and promotes the mortality of fungal-infected locusts.

Results

M. acridum infection results in dysbiosis of locust symbiotic microbiota

To investigate the interactions between *M. acridum*, a host-specific entomopathogenic fungus, and the symbiotic bacteria of migratory locusts, we initially conducted a dynamic analysis of both the fungal and symbiotic bacterial loads in the host. Given that *M. acridum* primarily colonizes the hemocoel of locusts during infection, we quantified the fungal and bacterial loads from hemolymph samples of locusts at specified intervals, ranging from 0 to 120 h post injection (hpi). The gene expression levels of the glyceraldehyde-3-phosphate dehydrogenase gene (*GPD*) and 16S ribosomal RNA (16S rRNA) were

used to determine the loads of *M. acridum* and symbiotic bacterial in vivo, respectively. Compared to 0 hpi, the *M. acridum* load significantly increased at 72 hpi and reached its peak at 120 hpi (Fig. 1A). Similarly, the bacterial load showed a substantial elevation at 96 and 120 hpi (Fig. 1B and Fig. S1A). To evaluate if interactions exist between the pathogenic fungus and symbiotic bacteria in locusts, we generated axenic locusts by continuously injecting antibiotics into the hemocoel (Fig. 1C). Post fungal infection, non-axenic locusts exhibited significantly higher mortality compared to axenic locusts (Log-rank test, $p < 0.05$) (Fig. 1D). The fungal load of *M. acridum* was approximately 1.5-fold higher in axenic locusts at 96 hpi compared to non-axenic locusts ($p = 0.026$, Mann–Whitney *U* test) (Fig. S1B). Furthermore, the expression levels of several antimicrobial genes (*Serpin*, *Lysozyme*, and *Attacin*) were significantly lower in axenic locusts compared to non-axenic locusts (Fig. S1C). These findings suggest that the proliferation of symbiotic bacteria within the host's hemocoel can influence the growth of *M. acridum*, amplify the host's inflammatory responses, and ultimately affect the host's survival.

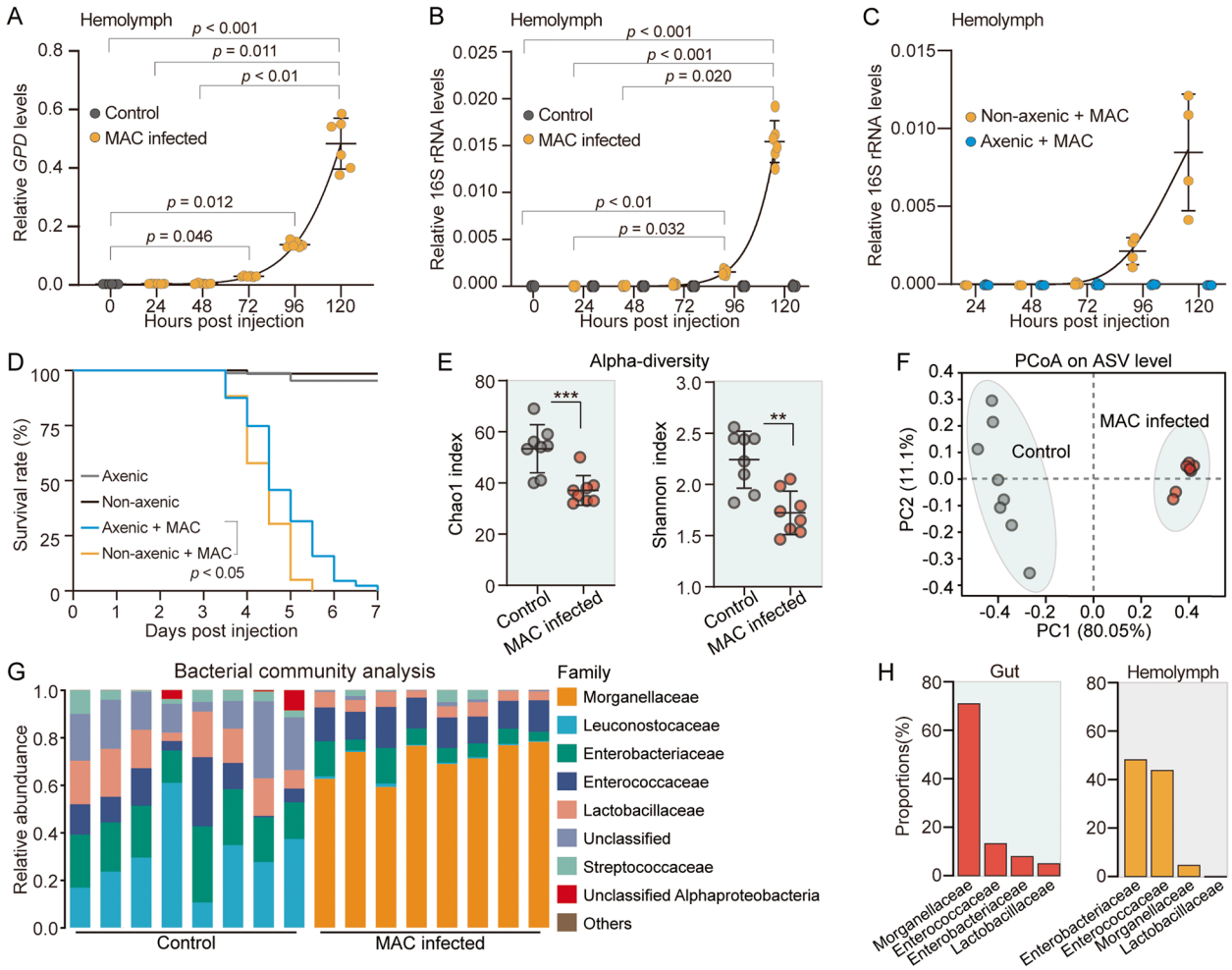

Fig. 1 *M. acridum* (MAC) infection causes dysbiosis of microbiota in locusts. **A** and **B** Quantifications of fungal (**A**) and total bacterial (**B**) loads in the hemolymph of locusts ($n = 6$, 10 individuals per replicate). Kruskal–Wallis test for multiple comparisons. Values are mean ± standard deviation (SD). Locusts injected with 0.1% Tween 80 serve as the control. **C** Quantifications of bacterial load in the hemolymph of axenic and non-axenic locusts after MAC injections ($n = 4$, 10 individuals per replicate). **D** Survival of axenic and non-axenic locusts after MAC injections ($n \geq 62$). Differences between axenic and non-axenic groups are analyzed using the Log-rank test. **E** Alpha diversity metrics (Chao1 and Shannon index) of bacterial communities in gut of locusts at amplicon sequencing variants (ASV)-level. Differences between control and MAC-infected groups were analyzed using the Mann–Whitney *U* test, with significant differences denoted as $^{**}p < 0.01$, and $^{***}p < 0.001$. **F** Principal coordinate analysis (PCoA) at the ASV-level showing the overall differences in gut microbial communities between control and MAC-infected locusts. **G** Alterations in microbial communities at the family level in the gut of control and MAC-infected locusts. **H** Bacterial abundance at the family level in hemolymph and gut of locusts after MAC infection

The impact of *M. acridum* infection on the locust's microbial composition was further examined. Given that the gut is one of the predominant sites for the colonization of the host's symbiotic bacteria, and recognizing that the symbiotic bacteria present in the hemocoel of the fungal-infected locusts originate, to a certain degree, from the gut, we investigated the dynamics of the symbiotic bacterial populations within the gut of the locusts at 0 (control) and 96 hpi with *M. acridum*, using deep sequencing of the 16S rRNA gene. Alpha diversity metrics revealed that *M. acridum* infection significantly reduced the richness (measured by Chao1 index, $p < 0.001$, Mann–Whitney U test) and evenness (measured by Shannon's index, $p = 0.002$, Mann–Whitney U test) of the microbial communities in the gut of the locusts (Fig. 1E). Principal coordinate analysis (PCoA) showed that the microbial communities in infected and non-infected locusts were primarily separated along the first principal coordinate, accounting for 80.05% of the variances (Fig. 1F). The analysis of the bacterial community at the family level indicated that the gut microbiota of non-infected locusts was predominantly comprised of Leuconostocaceae, Enterobacteriaceae, Enterococcaceae, Lactobacillaceae, and Streptococcaceae. However, at 96 hpi, Leuconostocaceae was substantially replaced by Morganellaceae. Consequently, the gut microbiota was primarily dominated by four bacterial families: Morganellaceae, Enterococcaceae, Enterobacteriaceae, and Lactobacillaceae (Fig. 1G). Moreover, since the bacterial load in the hemolymph of locusts significantly increased after fungal infection, the compositions of microbial communities in the hemolymph of fungal-infected locusts were further analyzed. Similar to those in the gut, the predominant bacterial families in the hemolymph at 96 hpi were Enterococcaceae, Enterobacteriaceae, Morganellaceae, and Lactobacillaceae (Fig. 1H). However, the microbial community structures displayed significant differences between these two tissues. The hemolymph was mainly occupied by the Enterococcaceae and Enterobacteriaceae, contributing to 43.7% and 48.1% of the proportions, respectively. In contrast, the gut was largely populated by the Morganellaceae, with a proportion of 70.8% (Fig. 1H). Thus, *M. acridum* infection reduces the microbial diversity and alters the microbial composition in locusts.

M. acridum infection induces dominance of some symbiotic bacteria in the hemocoel

To identify the species of the predominant symbiotic bacteria induced by *M. acridum* infection, the culturable bacteria from the hemocoel were isolated. Hemolymph from *M. acridum*-infected locusts was collected, spread onto Luria broth (LB) and Man Rogosa and Sharpe (MRS) plates, and incubated to allow bacterial growth. Isolated single bacterial colonies were identified through PCR amplification of the 16S rRNA gene using universal primers 27F and 1492R. Six predominant bacteria were ultimately identified, including *Enterococcus faecalis* and *Enterococcus gallinarum* from the Enterococcaceae family, *Proteus mirabilis* from the Morganellaceae family, *Weissella confusa* from the Lactobacillaceae family, and *Enterobacter hormaechei* and *Klebsiella aerogenes* from the Enterobacteriaceae family (Fig. 2A). Quantitative real-time PCR (q-PCR) results confirmed that the 16S rRNA genes of these six species were either nearly undetectable or maintained at extremely low levels in the hemolymph of noninfected locusts. In contrast, at 96 hpi with *M. acridum*, there was a significant increase in bacterial load within the hemolymph (Fig. 2B). Additionally, increases in the abundance of *E. faecalis*, *E. gallinarum*, *P. mirabilis*, and *K. aerogenes* in the hemocoel of locusts post-*M. acridum* infection were further corroborated by long-read sequencing at the species level (Table S1). When *M. acridum* and the predominant symbiotic bacteria were co-cultured on LB or MRS agar plates, no apparent antagonistic effects were observed between *M. acridum* and the bacterial isolates (Fig. S2). Therefore, the predominant symbiotic bacteria induced by *M. acridum* infection exhibit no antagonistic effects on fungal growth.

The predominant symbiotic bacteria, *E. faecalis* and *P. mirabilis*, have the potential to transform into opportunistic pathogens

To assess the potential impact of the predominant symbiotic bacteria on the survival of locusts, we individually injected 5×10^5 colony-forming units (CFUs) of each bacterial species into the hemocoel of 6 separate groups of locusts. The results showed that only *E. faecalis*, *P. mirabilis*, and *K. aerogenes* caused significant increases in locust mortalities. Notably, *E. faecalis* and *P. mirabilis* induced mortalities of the locust up to 93.1% and 79.3% within 2 days, respectively (Fig. 2C). Furthermore, we observed rapid proliferation of *E. faecalis* and *P. mirabilis* within 24 h post-injection into the locust's hemocoel (Fig. S3A). Absolute quantification results showed that *E. faecalis* and *P. mirabilis* were detectable in the gut of uninfected locusts, with mean 16S rRNA gene copy numbers of $1.67 \times 10^7 \pm 6.31 \times 10^6$ and $2.99 \times 10^8 \pm 1.23 \times 10^8$ per mL of gDNA, respectively, and proliferated extensively following fungal infection (Fig. S3B). Therefore, *E. faecalis* and *P. mirabilis* are commensal bacteria that reside in the locust gut. Should their expansion within the hemocoel become unregulated, they may transform into opportunistic pathogens, leading to the rapid death of the host.

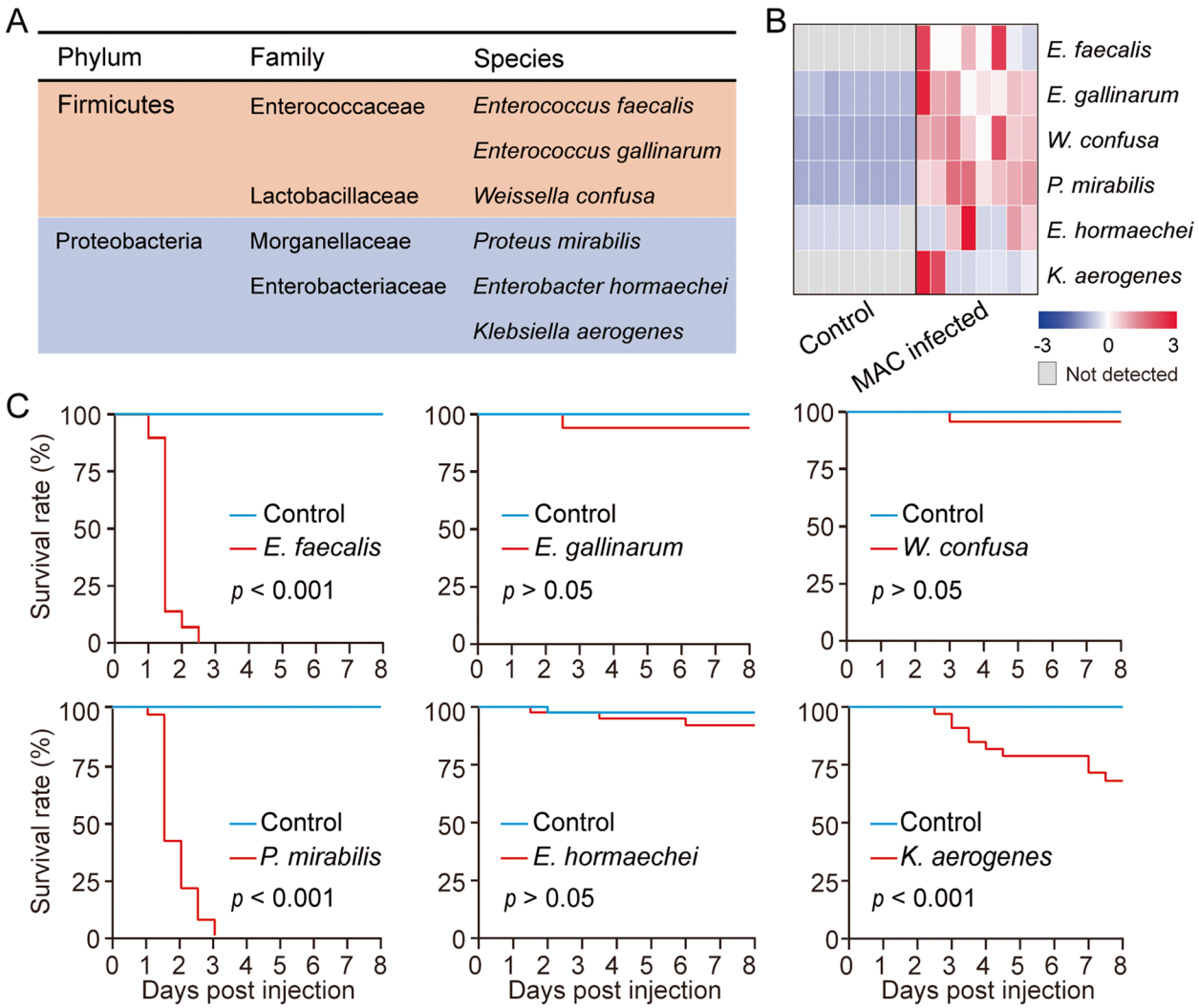

Fig. 2 Transformation from symbiotic bacteria to opportunistic pathogens results in the death of locusts. **A** Culturable bacterial isolates derived from hemolymph samples of locusts at 96 h post-infection (hpi) with MAC. **B** Quantification of relative bacterial levels in locusts' hemolymph at 96 hpi with MAC using specific 16S rRNA primers ($n = 8$; 5 locusts per replicate). The heatmap illustrates log2 fold-change values. **C** Survival of locusts ($n = 30$) after injection of 5×10^5 colony-forming units (CFUs) of bacterial isolates into the hemocoel. Locusts injected with H_2O serve as controls. Differences between the control and bacteria-injected groups are analyzed using the Log-rank test

In one-quarter-strength Sabouraud dextrose (¼SDAY) liquid medium, a high bacterial load (over 3.0 OD_{600}) of *E. faecalis* and *P. mirabilis* significantly inhibited *M. acridum* growth (Fig. S3C). These results imply that excessive proliferations of the predominant symbiotic bacteria have the potential to negatively impact fungal growth. Therefore, we speculate that to effectively exploit host resources, *M. acridum* must develop strategies to limit the rapid proliferation of these bacteria.

MaCFEM1 is indispensable for *M. acridum* hyphal growth when exposed to bacteria

To elucidate the direct interactions between *M. acridum* and bacteria in vivo, we compared the gene expression profiles of *M. acridum* in both axenic and non-axenic locusts. Total RNA was extracted from the hemolymph of *M. acridum*-infected locusts and subjected to RNA sequencing (RNA-seq) (Fig. 3A). After filtering, correcting, and aligning the raw data to the

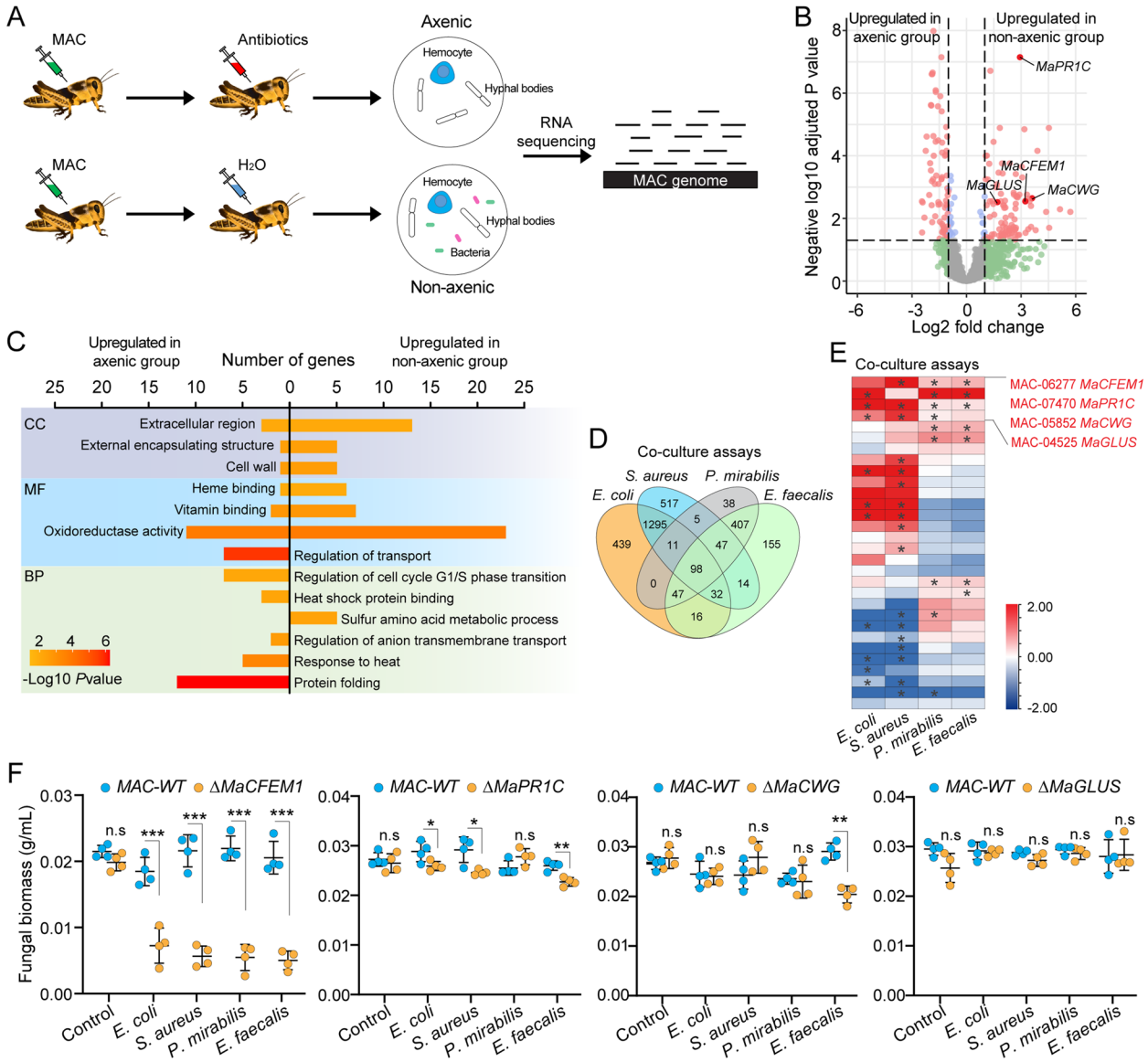

Fig. 3 MaCFEM1 is crucial for the colonization of MAC in the presence of symbiotic bacteria. **A** Experimental procedure for analyzing MAC gene expression in axenic and non-axenic locusts. **B** Volcano plot showing the overall gene expression pattern of MAC in axenic and non-axenic locusts. **C** GO enrichment analysis of differentially expressed genes (DEGs), displaying only GO terms with a *p* value < 0.05. CC, MF, and BP represent cellular components, molecular functions, and biological processes, respectively. **D** The Venn diagram shows the shared and unique DEGs induced by different bacterial species under fungal-bacterial co-culture conditions. **E** Gene expression patterns of the candidate DEGs under co-culture conditions. The heat map signal indicates log2 fold-change values of co-cultured groups relative to the control group. MAC cultured alone in ¼SDAY liquid medium serves as the control. Treatments with adjusted *p* value < 0.05 are denoted by *. **F** Fungal biomass of WT and mutant strains when co-cultured with *E. faecalis*, *P. mirabilis*, *S. aureus*, and *E. coli* in ¼SDAY liquid medium, respectively ($n = 4$). Values are presented as mean ± SD., and differences between WT and mutant strains were analyzed using Student's *t*-test, with significant differences denoted as $^{*}p < 0.05$, $^{**}p < 0.01$, $^{***}p < 0.001$. *MaPR1C*, *MaCWG*, and *MaGLUS* are gene names for subtilisin-like serine protease PR1C, antigenic cell wall galactomannoprotein, and alpha-glucosidase, respectively

genome of *M. acridum*, we identified 198 differentially expressed genes (DEGs) with an adjusted *p*-value lower than 0.05. Among these DEGs, 102 were upregulated in non-axenic locusts and 96 in axenic locusts (Fig. 3B). Gene Ontology (GO) enrichment analysis indicated that the DEGs highly expressed in axenic locusts were primarily involved in protein folding, anion transport, and mitosis. In contrast, DEGs highly expressed in non-axenic locusts were mainly associated with nutrient binding or acted as components of the cell wall,

external encapsulating structures, and the extracellular region (Fig. 3C).

Through whole genome scanning of *M. acridum*, we did not observe genes encoding proteins with high similarity to fungal antimicrobial peptides. Instead, we identified six genes in *M. acridum* encoding proteins belonging to the lysozyme superfamily, including two genes encoding proteins with family 25 glycoside hydrolase domains. However, these genes exhibited extremely low expression levels under both axenic and non-axenic conditions (Fig. S4). Furthermore, the only gene cluster systematically upregulated in non-axenic locusts was responsible for swainsonine biosynthesis (Fig. S5A–C). Swainsonine, an indolizidine alkaloid and the main toxin in locoweeds, is produced by some toxic legumes and fungi [38, 39]. However, an inhibition zone assay demonstrated that it did not have a discernible effect on bacterial growth (Fig. S5D). Therefore, when confronted with bacteria in vivo, *M. acridum* upregulate a variety of proteins primarily involved in the extracellular region, cell wall components, and nutrient binding.

Thirty DEGs, encoding proteins involved in the extracellular region, cell wall components, and nutrient binding, were pinpointed as candidate genes (Table S2). To further investigate the involvement of these biological processes in fungal-bacterial interactions and to minimize the potential influences of in vivo factors introduced by the locusts, we conducted co-culture assays in vitro. Conidia of *M. acridum* were cultured in ¼ strength SDAY liquid medium for 24 h either alone, or in co-culture with *E. faecalis*, *P. mirabilis*, *Staphylococcus aureus*, and *Escherichia coli*, respectively. All these bacteria grow well in ¼ strength SDAY liquid medium when cultured alone (Fig. S6). Gene expression profiles for *M. acridum* were generated through RNA-seq analysis. According to the Venn diagram, approximately 37% of DEGs were specific to a single bacterial treatment, while a mere 3% were responsive to all four bacterial species (Fig. 3D). To identify genes that interact with a wide range of bacteria, we focused on DEGs induced by at least three of the bacterial species mentioned above. In comparison to the control group, the expressions of MAC_06277, MAC_07470, MAC_05852, and MAC_04525 among the thirty candidates were significantly induced by at least three of the aforementioned bacterial species (Fig. 3E). These genes encode the proteins MaCFEM1, Subtilisin-like serine protease PR1C, Antigenic cell wall galactomannoprotein (MaCWG), and Alpha-glucosidase (MaGLUS), respectively. To further investigate the involvement of these genes in fungal-bacterial interactions, null mutant strains were generated (Fig. S7). Compared to the wild-type strain (WT), the mutant strains did not exhibit any obvious growth defects when cultured alone. However, under co-culture conditions, only the biomass of the *MaCFEM1* knockout strain (*ΔMaCFEM1*) was extensively repressed by at least 60% in the presence of all tested bacterial isolates. In contrast, the biomasses of the other mutant strains (Δ*MaPR1C*, *ΔMaCWG*, and *ΔMaGLUS*) exhibited either no significant changes or were only slightly reduced (Fig. 3F). Therefore, *MaCFEM1* is the crucial effector for *M. acridum* growth when confronted with bacterial challenges.

MaCFEM1, a fungal *iron*-binding protein, functions in *iron* uptake

To investigate the possible function of MaCFEM1, we conducted structural and functional analyses. Based on the gene and amino acid sequences of MaCFEM1, we modeled the structure of the protein. MaCFEM1 contains a Common in Fungal Extracellular Membrane (CFEM) domain (Fig. 4A), the three-dimensional structure of which was generated using RoseTTAFold [40] (Fig. S8A). This domain is comprised by 6 alpha-helices which are held together by 4 disulfide bonds. Additionally, an aspartic acid residue at position 45 (D45) forms an axial ligand, which is structurally similar to that in Csa2 (Secreted hemophore CSA2), a CFEM protein in *Candida albicans* [41]. We then conducted sequence alignment between MaCFEM1 and CFEM proteins in *C. albicans*, including Csa2, Pga7 (GPI-anchored hemophore PGA7), and Rbt5 (GPI-anchored hemophore RBT5). The CFEM domain of MaCFEM1 is characterized by a conserved pattern of eight cysteine residues with specific spacing ($Cx_3Cx_{10-12}Cx_{6-7}CxCx_{11-14}Cx_4Cx_{15-16}C$) along with a conserved aspartic acid residue (D45) (Fig. S8B). Given the high structural similarity of MaCFEM1 with the CFEM proteins in *C. albicans*, we suspected the functions of MaCFEM1 could be involved in iron assimilation [41]. Thus, we tested the expression levels of MaCFEM1 under iron-deficient conditions. Compared to the control group (cultured in ¼SDAY liquid medium), *MaCFEM1* showed significant upregulation in response to iron deficiency ($p < 0.001$, Mann–Whitney *U* test) (Fig. 4B). Furthermore, no significant differences in fungal growth were observed between the WT and *ΔMaCFEM1* under iron-sufficient conditions. However, under iron-deficient conditions, *ΔMaCFEM1* displayed a marked reduction in growth (Fig. 4C). We then expressed MaCFEM1 in the Origami-B *E. coli* strain that permits disulfide-bond formation within the bacterial cytoplasm (Fig. 4D). The binding affinity of MaCFEM1 on iron was measured using isothermal titration calorimetry, with a mean dissociation constant from three independent experiments as 0.67 ± 0.34 μM (Fig. 4E). Therefore, MaCFEM1 is an iron-binding protein that enables *M. acridum* to assimilate iron under iron-deficient conditions.

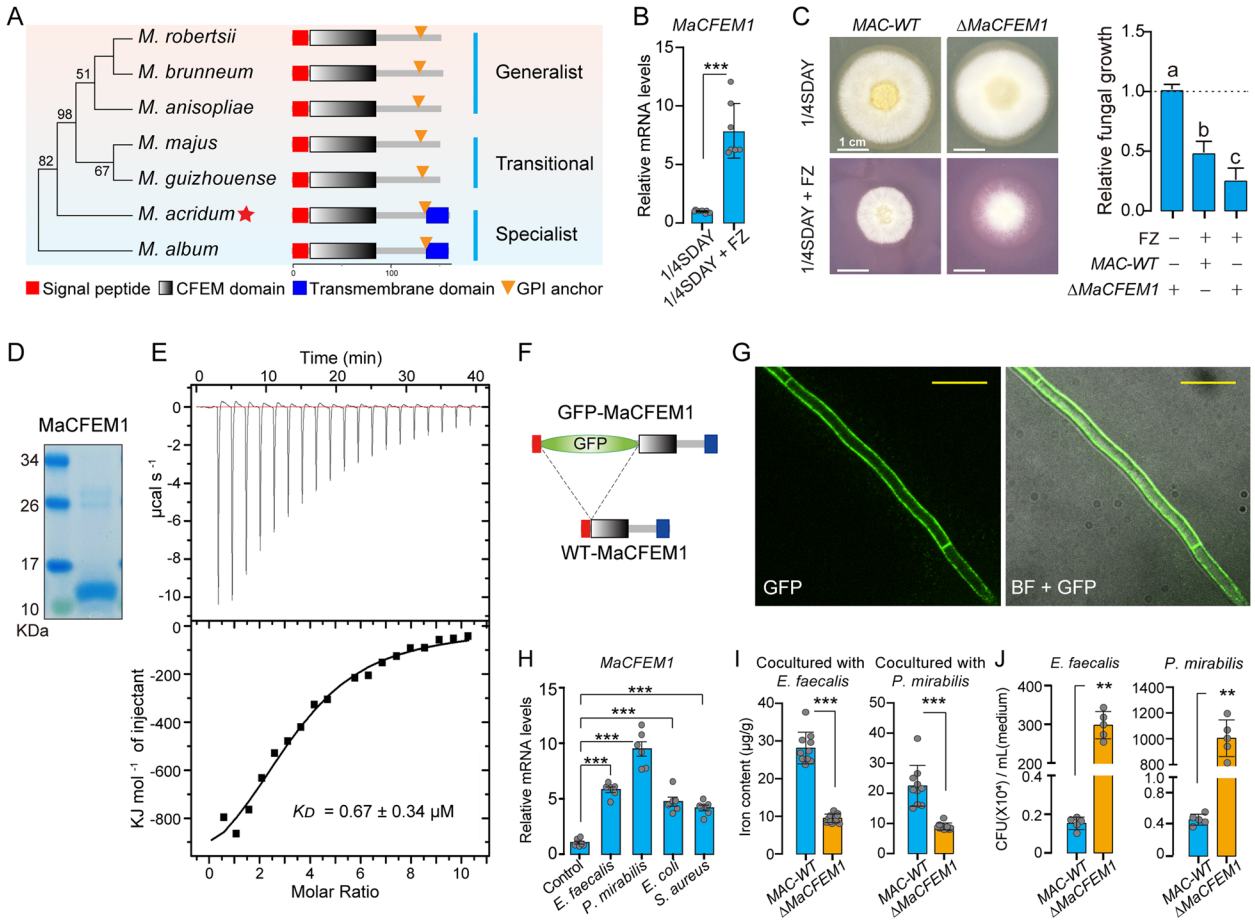

Fig. 4 MaCFEM1 is an iron-binding protein participating in iron uptake and competition. **A** Phylogenetic tree illustrates the relationship among MaCFEM1 orthologues in different *Metarhizium* species. *M. acridum* and *M. album* are host-specialists, while *M. robertsii*, *M. brunneum*, and *M. anisopliae* are host-generalists. *M. majus* and *M. guizhouense* are transitional species. The phylogenetic tree was conducted using maximum likelihood method. **B** Gene expression profile of *MaCFEM1* under normal and iron-deficient conditions ($n = 7$). FZ is the abbreviation for Ferrozine, an iron chelator. **C** Growth of WT and *ΔMaCFEM1* under iron-deficient conditions. Relative fungal growth was calculated by normalizing against the area of fungal colonies of the WT grown on the ¼SDAY agar plates. **D** In vitro expression and purification of MaCFEM1. **E** Isothermal titration calorimetry analysis for the interaction between Mcfem1 and ferric iron. In three independent experiments, titrating 100 μM proteins into a solution of 10 μM ferric iron resulted in MaCFEM1-Fe^{3+} $N = 3.03 \pm 0.86$ sites, $Ka = 1.69 \times 10^6 \pm 8.329 \times 10^5$ $M-1$, and $\Delta H = -1.17 \times 10^6 \pm 7.935 \times 10^5$ J/mol. **F** Schematic diagram for the structure of GFP-MaCFEM1. **G** Subcellular localization of GFP-MaCFEM1 in MAC hyphae. Scale bar: 10 μm. **H** MAC upregulates *MaCFEM1* expressions when co-cultured with *E. faecalis*, *P. mirabilis*, *E. coli*, and *S. aureus*, respectively ($n = 6$). MAC cultured alone in ¼SDAY liquid medium is set as the control. **I** Iron content per gram of mycelium ($n = 10$). **J** CFU of *E. faecalis* and *P. mirabilis* per milliliter of liquid medium under co-culture conditions ($n = 5$). Values are presented as mean ± SD, One-way ANOVA with Bonferroni's test for multiple comparisons (C and H), Mann–Whitney *U* test (**B**, **I**, and **J**) for pairwise comparisons. Significant differences are denoted by $^{***}p < 0.001$ or by different letters

The sequences and structures of MaCFEM1 orthologous genes were further compared across several *Metarhizium* species. In addition to the CFEM domain, MaCFEM1 also possesses a C-terminal glycosylphosphatidylinositol (GPI) anchor and a transmembrane domain. Only the host-specialist species, *M. acridum* and *M. album*, in the genus *Metarhizium* were found to possess MaCFEM1 orthologs with a transmembrane domain (Fig. 4A). To determine the subcellular localization of MaCFEM1, we inserted green fluorescent protein (GFP) tag in a position between the signal peptide and CFEM domain, generating a GFP-MaCFEM1 fusion protein (Fig. 4F). After 72 h of in vitro culture, strong green fluorescence signals of GFP-MaCFEM1 were observed at the cell surface of growing hyphae (Fig. 4G). Therefore, MaCFEM1 is possibly a transmembrane or anchoring protein located at the cell surface of *M. acridum*.

M. acridum employs MaCFEM1 for constraining bacterial overgrowth by restricting iron availability

To test the function of MaCFEM1 in fungal-bacterial interactions, we conducted in vitro co-culture assays. Firstly, the expression levels of *MaCFEM1* were examined when *M. acridum* was co-cultured with *E. faecalis*, *P. mirabilis*, *S. aureus*, and *E. coli*, respectively. Compared to the control group, *M. acridum* cultured alone, the expression of *MaCFEM1* increased by approximately fivefold when induced by the bacteria (Fig. 4H). Subsequently, iron uptake mediated by MaCFEM1 was assessed by measuring the iron content of *M. acridum* hyphae under fungal-bacterial co-culture conditions. The iron concentration in the Δ*MaCFEM1* hyphae was found to be reduced by approximately 50% and 60%, compared to the WT, when co-cultured with *E. faecalis* and *P. mirabilis*, respectively (Fig. 4I). Furthermore, co-culturing with the Δ*MaCFEM1* resulted in a substantial increase in the bacterial load of *E. faecalis* and *P. mirabilis*, approximately 1500-fold and 2500-fold, respectively, compared to co-culturing with the WT (Fig. 4J). While the absence of MaCFEM1 does not affect the fundamental iron uptake of *M. acridum*, its deficiency compromises the fungus's ability to compete for iron with bacteria. This shift in iron allocation gives bacteria a chance to access a greater supply of iron, resulting in their extensive proliferation.

Given the acquisition of iron through CFEM proteins operates as a relay system, which is facilitated by the collaborative efforts of various CFEM proteins [41, 42]. We conducted a systematic analyzation of CFEM genes in *M. acridum* and finally identified 10 CFEM genes based on the genome-wide scanning (Fig. S9A). Their CFEM domains are highly conserved in the eight cysteine residues (Fig. S9B). In addition to *MaCFEM1*, *MaCFEM3*, *5*, *6*, and *10* also exhibited significant upregulations in response to iron deficiency (Fig. S9C). Additionally, the expression patterns of CFEM genes in *M. acridum* were examined both in vitro and in vivo upon bacterial stimulations. According to the RNA-seq data, in vitro co-culture conditions resulted in a general upregulation of CFEM genes in response to bacterial induction, except for *MaCFEM2*, *5*, and *10* (Fig. S9D). However, only *MaCFEM1* exhibited a dramatic upregulation in non-axenic locusts compared with axenic locusts, while the remaining CFEM genes were less sensitive to bacterial induction in vivo (Fig. S9E). Thus, the acquisition of iron in *M. acridum* is possibly conducted by collaborations of multiple CFEM proteins. When it comes to microbial iron-competitions in the host, MaCFEM1 may occupy a pivotal position.

Locusts infected with *ΔMaCFEM1* died rapidly due to extensive bacterial proliferation

We evaluate the effect of MaCFEM1-mediated fungal-bacterial interactions on the host for the potential application in pest control. The expression of *MaCFEM1* in *M. acridum*-infected locusts was quantified through q-PCR at 96 hpi. Results showed a significant upregulation of *MaCFEM1* in non-axenic locusts compared to the axenic ones (Fig. 5A). Then, we assessed the pathogenicity of WT and *ΔMaCFEM1* by comparing their respective impacts on locust mortality. In non-axenic locusts, both injection and topical infection assays demonstrated that *ΔMaCFEM1* infection caused significantly higher mortality compared to WT infection (Log-rank test, $p < 0.001$ for injection, and $p < 0.01$ for topical infection) (Fig. 5B). On the contrary, no significant difference in the mortalities of axenic locusts was observed while infected with these fungal strains (Fig. 5C).

We then measured the bacterial and fungal burdens in locusts following infection with the WT and *ΔMaCFEM1* at 96 hpi (Fig. 5D and E). In the hemolymph of non-axenic locusts, infections with *ΔMaCFEM1* resulted in a dramatic elevation of bacterial load compared to that with the WT ($p < 0.001$, Student's *t*-test). Meanwhile, the fungal load of *ΔMaCFEM1* was 50% lower than that of the WT ($p < 0.01$, Mann–Whitney *U* test) (Fig. 5D and Fig. S10). In axenic locusts, bacterial 16S rRNA was scarcely detectable by q-PCR following *M. acridum* infection, and the fungal loads exhibited no significant differences between infections with the WT and *ΔMaCFEM1* ($p = 0.24$, Mann–Whitney *U* test) (Fig. 5D). Furthermore, the presence of *E. faecalis* and *P. mirabilis* 16S rRNA genes was confirmed only in the hemolymph of non-axenic locusts. In these locusts, the *ΔMaCFEM1* infection resulted in a fourfold increase in *E. faecalis* load ($p < 0.01$, Mann–Whitney *U* test) and a tenfold increase in *P. mirabilis* load ($p < 0.01$, Mann–Whitney U test), when compared to the WT infection (Fig. 5E). To determine if the elevated bacterial load observed in locusts infected with Δ*MaCFEM1* was due to increased iron availability in the hemolymph, we quantified the iron concentrations. We noted an approximate 1.5-fold rise in the iron levels in the hemolymph of locusts infected with Δ*MaCFEM1* relative to those infected with the WT (Fig. 5F). Additionally, in vitro cultivation assays demonstrated the importance of a sufficient iron supply for bacterial proliferation (Fig. S11). Thus, Infection with *ΔMaCFEM1* allows the predominant symbiotic bacteria to access abundant iron resources. As a result, certain bacteria proliferate rapidly and evolve into opportunistic pathogens, significantly accelerating the death of locusts.

To determine if the *ΔMaCFEM1*-infected locusts primarily died due to bacterial proliferation, we quantified

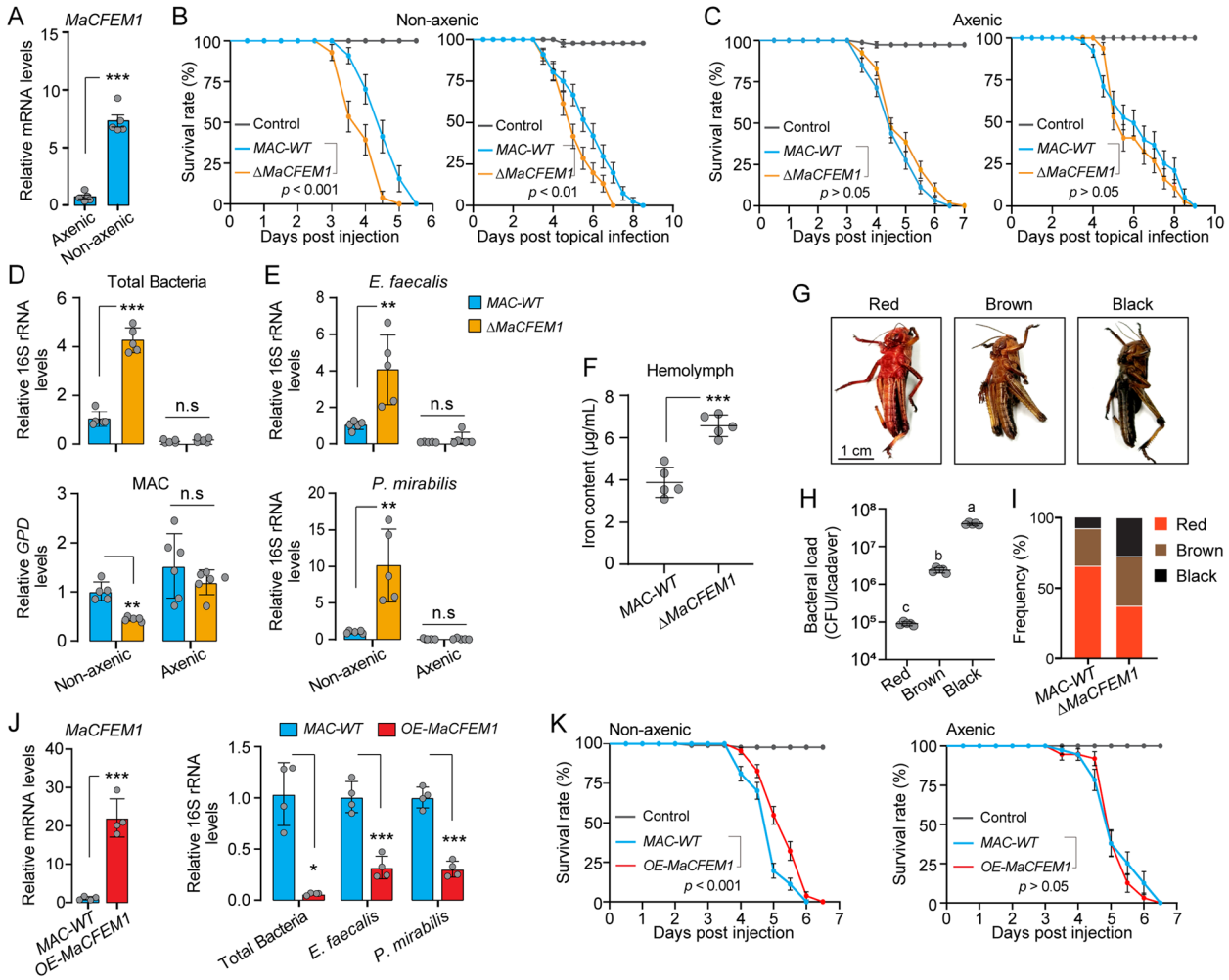

Fig. 5 *ΔMaCFEM1* infection causes uncontrolled proliferation of opportunistic bacteria, accelerating locust death. **A** Expression of MaCFEM1 under axenic and non-axenic conditions ($n = 5$, 8 locusts/replicate). **B** and **C** Survival rate of non-axenic and axenic locusts following WT and *ΔMaCFEM1* injections or topical infections ($n \geq 30$). Locusts treated with 0.1% Tween 80 were used as controls. **D** Quantification of total bacterial and MAC fungal loads in non-axenic and axenic locusts at 96 hpi. **E** Quantification of *E. faecalis* and *P. mirabilis* loads in non-axenic and axenic locusts at 96 hpi ($n \geq 5$, 8 locusts/replicate). **F** Iron content in hemolymph of locusts at 96 hpi with WT and *ΔMaCFEM1* ($n = 5$, 20 individuals/replicate). **G** Cadavers of MAC-infected locusts were categorized into three types based on body color: red, brown, and black. **H** Bacterial load in different cadavers ($n = 5$, 8 cadavers/replicate). **I** Ratio of different cadavers calculated following WT and *ΔMaCFEM1* infections ($n \geq 90$). **J** Expression levels of MaCFEM1 in WT and *MaCFEM1* overexpression strain (*OE-MaCFEM1*) in vivo, and bacterial load at 96 hpi with WT and *OE-MaCFEM1* ($n = 4$, 8 locusts/replicate). **K** Survival rate of locusts after WT and *OE-MaCFEM1* infections ($n \geq 60$). Locusts injected with 0.1% Tween 80 serve as the control. **A**, **D**, **E**, **I**, and **J** Values represent mean ± SD. Pairwise comparisons were performed using Student's *t*-test or Mann–Whitney *U* test, and significant differences are indicated by $^{**}p < 0.01$, $^{***}p < 0.001$. n.s represents no significant differences. **H** One-way ANOVA with Bonfferroni's test for multiple comparisons. Values are mean ± SD, significant differences are denoted by different letters. **K** Log-rank test for survival dynamics analysis

bacterial colonies in locust cadavers using the spread-plate method after infections with the WT and *ΔMaCFEM1*, respectively. The cadavers of *M. acridum* infected locusts were categorized into three types of body color: red, brown, and black (Fig. 5G). Red cadavers had minimal bacterial colonies that were barely detectable on plates after a 10,000-fold dilution. In contrast, black cadavers harbored the highest number of bacterial colonies, with brown cadavers closely behind (Fig. 5H). In cadavers infected with the WT ($n = 90$), 65% were red, 27% were brown, and 8% were black. However, in cadavers infected with *ΔMaCFEM1* ($n = 94$), the percentage of red cadavers decreased to 37%, while the percentages of brown and black cadavers increased to 35% and 28%, respectively ($\chi^2 = 18.41$, $df = 2$, $p < 0.001$) (Fig. 5I). Consequently, locusts infected with *ΔMaCFEM1* primarily died from the prevalence of opportunistic bacteria, which ultimately dominated their cadavers.

To further confirm the iron-competitive role of MaCFEM1 in bacterial-fungal interactions in vivo, we created an *MaCFEM1* overexpression strain (*OE-MaCFEM1*). This led to a 20-fold increase in *MaCFEM1* expression levels in the *OE-MaCFEM1* compared to the WT in vivo (Fig. 5J). Moreover, the bacterial loads of total bacteria, *E. faecalis*, and *P. mirabilis* in the locust hemolymph after *OE-MaCFEM1* infection were significantly lower than those after WT infection (Mann–Whitney U test for comparation of total bacterial load; Student's *t*-test for *E. faecalis* and *P. mirabilis* loads) (Fig. 5J). Additionally, *OE-MaCFEM1* infection caused significantly lower mortality in non-axenic locusts, but not in axenic locusts, compared to WT infection (Log-rank test, $p < 0.001$) (Fig. 5K). Thus, the overexpression of *MaCFEM1* in *M. acridum* suppresses the growth of the predominant symbiotic bacteria in the locust hemocoel, resulting in a prolonged lifespan of locusts after fungal infection. Therefore, MaCFEM1 plays a crucial role in constraining the growth of symbiotic bacteria in the host by limiting the availability of free iron. The microbial interactions mediated by MaCFEM1 ultimately determine the host's mortality (Fig. 6).

Discussion

This study reveals a complex interaction between an entomopathogenic fungus and symbiotic bacteria in locusts, characterized by commensal and competitive dynamics. We observed that in the advanced stages of *M. acridum* infection, the loads of both fungus and bacteria within the locust's hemocoel reach their peak concentrations. Concurrently, it is likely that, *M. acridum* selectively induces the dominance of some symbiotic bacteria that do not exhibit antagonistic effects against the fungus, thereby establishing a bacterial environment compatible with the fungal growth. Infections by entomopathogenic

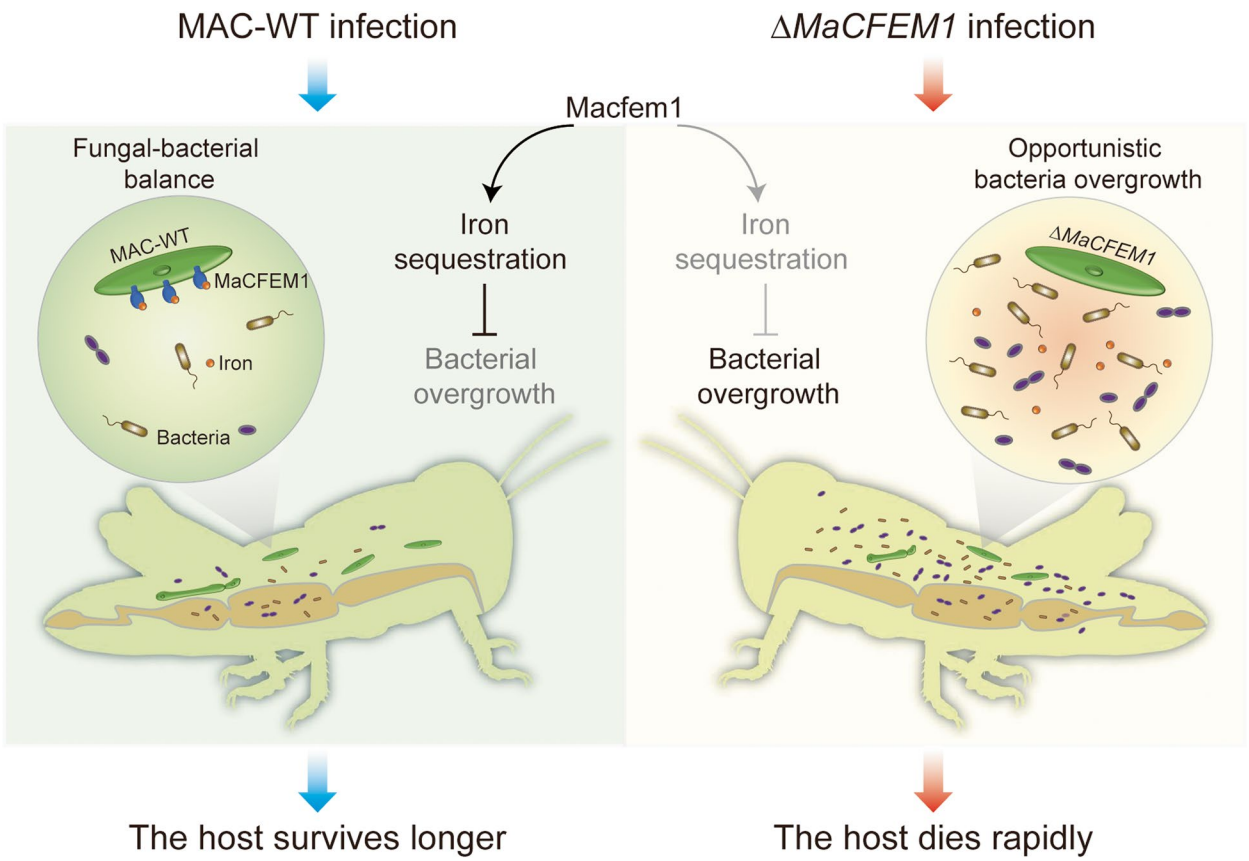

Fig. 6 The proposed model demonstrates that disruption of the iron competition-driven microbial equilibrium can trigger symbiotic bacteria to transform into opportunistic pathogens, thereby elevating host mortality. Infection by *M. acridum* disrupts the composition of the locust microbiota, leading to the dominance of some symbiotic bacteria and prompting their migration from the gut to the hemocoel. Meanwhile, the fungus maintains a delicate balance with these bacteria in the hemocoel by restraining their overgrowth, thereby efficiently exploiting host resources. In the presence of bacteria, *M. acridum* upregulates the iron-binding protein MaCFEM1, which sequesters iron, thus restricting bacterial access to iron. Knockout of *MaCFEM1* removes these fungal-imposed limitations on bacterial iron acquisition, resulting in unregulated bacterial proliferation. Consequently, locusts infected with the Δ*MaCFEM1* exhibit high mortality and shortened lifespans due to the uncontrolled proliferation of opportunistic bacteria

fungi inevitably lead to the disruption of the host's microbiota and the proliferation of some symbionts in the body cavity, intensifying microbial interactions in the insect host. Many symbiotic bacteria that inhabit in the insect are able to antagonize pathogenic fungi by producing a range of antifungal compounds [16–18]. Therefore, for successful colonization of the host's internal environment, pathogenic fungi must inhibit the growth of any antagonistic symbiotic bacteria [43]. Nonetheless, synthesizing antimicrobial substances could be energetically expensive and might slow the fungal growth towards sporulation, potentially impairing reproductive success [37]. Thus, supporting the dominance of non-antagonistic bacteria and coexisting with these bacteria means a sophisticated adaptive strategy of pathogenic fungi. While much of the prevailing research has been focused on the antagonistic relationships between symbiotic bacteria and entomopathogenic fungi, our study sheds light on a delicate equilibrium.

In the advanced stages of fungal infection, host immune dysregulation and reduced pathogen clearance efficacy become prominent, with microbial interactions emerging as a critical factor shaping the growth dynamics of both fungi and bacteria. Our findings reveal that at 96 hpi, the locust upregulates various antimicrobial genes in response to fungal and bacterial proliferation within the hemocoel. However, the expression of these genes proves insufficient to effectively inhibit pathogen growth. Both fungi and bacteria reach a plateau phase at 120 hpi. Previous studies have demonstrated that during the early stages of fungal infection, host-produced antimicrobial peptides can effectively suppress the proliferation of opportunistic bacteria [21]. However, as mycosis progresses, entomopathogenic fungi release multiple of secondary metabolites and secreted proteins that impair the host's immune system, leading to immune dysregulation [44, 45]. Consequently, the compromised immune system fails to effectively control pathogen growth, thereby elevating microbial interactions to a determinant of pathogen load and host mortality.

The commensal gut bacteria *E. faecalis* and *P. mirabilis* are identified as potential opportunistic pathogens in locusts. Our research demonstrates that, while *E. faecalis* and *P. mirabilis* can reside within the gut of healthy locusts without causing harm, their direct injection into the locust's hemocoel leads to swift death. This suggests that these symbionts can transform into opportunistic pathogens when they proliferate uncontrollably within the hemocoel. Host microbes usually act as protectors against the invasion of pathogens, but under some circumstances, they may directly or indirectly facilitate the onset of disease caused by invading pathogens [46]. The transition of commensal bacteria towards pathogenicity is influenced by changes in the host's internal environment, resulting in the infiltration of bacteria into insect tissues where they should not normally be present [47–49]. In insects, *E. faecalis* and *P. mirabilis* are both commensal bacteria that colonize a variety of tissues, including the gut, epicuticle, or salivary glands [23, 50, 51]. *E. faecalis* colonizing the epicuticle of *Drosophila* can prevent *B. bassiana* infection by inhibiting the germination and penetration of fungal spores [23]. In the midgut of *Galleria mellonella* larvae, *E. faecalis* proliferates significantly during *Cordyceps militaris* mycosis and exhibits notable antagonistic effects on *C. militaris* growth [52]. However, fungal pathogenesis can facilitate the translocation of bacteria from the gut, cuticle, or trachea into the hemolymph. If *E. faecalis* and *P. mirabilis* migrate to the hemocoel and undergo unrestricted growth, they may cause disease or death. For instance, *Manduca sexta* larvae die rapidly after the direct injection of *E. faecalis* into the hemocoel [48]. Additionally, the ureases secreted by *P. mirabilis* exhibited strong neurotoxicity to insects [53].

In this study, we discovered that one of the strategies of *M. acridum* to constrain bacterial overgrowth is restricting iron availability. Although the predominant symbiotic bacteria do not antagonize *M. acridum* growth, they still compete with the fungus for host resources. Moreover, we found that in the presence of bacteria, *M. acridum* upregulates numerous biological processes involved in nutrient assimilation. Among these, *M. acridum* establishes dominance over bacteria through iron competition. Iron is one of the most important metals for microorganisms due to its involvement in a range of vital biological processes [54]. However, high concentrations of iron are toxic to cells, therefore the free iron is maintained in a low level within animal hosts [55]. The vast majority of iron in mammals is complexed with hemoproteins or the iron-storage protein ferritin [56]. The iron in insects is primarily intracellular or ferritin-bounded [57]. Additionally, iron-withholding is also employed by mammals and insects as a way of nutritional immunity to limit the availability of iron to invading microbes [58, 59]. Thus, possessing a superior capacity to acquire iron is crucial for a microorganism to gain a competitive edge in the host.

Our study demonstrates that *M. acridum* competes for iron with bacteria by expressing MaCFEM1. Higher levels of MaCFEM1 expression allow *M. acridum* to monopolize iron resources, significantly inhibiting bacterial growth. In contrast, removing the MaCFEM1 coding gene does not interfere with the fundamental iron uptake of *M. acridum* but impairs its competitive edge over bacteria for iron. The absence of MaCFEM1 leads to a 50–60% reduction in the fungus's iron absorption,

enhancing the iron availability for bacterial growth. Consequently, locusts infected with the *ΔMaCFEM1* primarily succumb to overwhelming opportunistic bacterial infections. MaCFEM1 belongs to the family of CFEM proteins, which is a group of fungal-specific proteins that are more abundant in pathogenic fungi compared to free-living fungi [60, 61]. These proteins have diverse functions in fungal biology, including maintaining cell wall integrity, facilitating adhesion, mediating host–pathogen interactions, acquiring nutrients, and responding to stress [62–65]. In *C. albicans*, CFEM proteins such as Csa2, Rbt5, and Pga7 act as heme receptors in a relay system, allowing the fungus to acquire iron from the iron-restricted environment in the mammalian host [41, 42, 66]. Moreover, the iron-assimilative role of CFEM proteins has also been reported in various other pathogenic fungi [67–69]. Most research illustrates that CFEM proteins directly target either the host's nutritional resources or defense systems. In our study, the overexpression and knockout of MaCFEM1 affected only the lifespan and mortality of non-axenic locusts, not axenic locusts. This suggests that MaCFEM1's role in iron assimilation is specifically involved in fungal-bacterial interactions. Therefore, this study provides an entirely new perspective on the function of CFEM proteins and underscores the importance of MaCFEM1-mediated microbial interactions for host survival. Furthermore, considering that locusts may utilize transferrin-mediated nutritional immunity to combat fungal infections, *M. acridum* also employs various iron uptake mechanisms, such as secreting siderophores, to interact directly with the host [70].

Antimicrobial peptides and certain secondary metabolites secreted by entomopathogenic fungi are known to play direct roles in inhibiting bacterial proliferation [22, 23]. However, our comprehensive genomic and transcriptomic analyses revealed the absence of genes encoding antimicrobial peptides in this *M. acridum* strain. Moreover, genes with potential antimicrobial functions, such as those encoding lysozymes, displayed extremely low expression levels in both axenic and non-axenic conditions. On the other hand, in the presence of bacteria, we observed significant upregulation of numerous enzymes potentially involved in secondary metabolite synthesis and secretion in *M. acridum*. These included members of the Major Facilitator Superfamily (MFS), ATP-binding cassette (ABC) transporter proteins, P450 enzymes, and glycosyl hydrolases (Table S3). These upregulations suggest that *M. acridum* may be capable of producing and secreting antimicrobial secondary metabolites in response to bacterial induction. Nevertheless, as previously mentioned, the process of fungal-bacterial interaction in the host is complex, requiring the involvement of multiple genes, pathways, and biological processes. From the perspective of nutrient allocation, this study proposes a competitive mechanism underlying the commensalism between pathogenic fungi and host symbiotic bacteria.

Our research may suggest a biological control method via exploiting the synergistic relationship between engineered pathogenic fungi and the host's symbiotic bacteria. By genetically modifying the entomopathogenic fungus, we shift the fungal-dominated microbial iron allocation, thereby facilitating the uncontrolled proliferation of symbiotic bacteria within host hemocoel during fungal infection. As a result, there is a significant reduction in the LT_{50} for the host. During infection, entomopathogenic fungi normally maintain a delicate balance between their growth, virulence, and interaction with bacteria, optimizing reproduction while preventing bacterial overgrowth to efficiently use host resources [37, 71]. This symbiotic equilibrium, however, unintentionally prolongs the lifespan of the host, which is counterproductive for pest control objectives that require rapid death and high mortality. To address this, we purposefully disrupted this balance, allowing opportunistic bacteria to thrive, which, in turn, leads to elevated host mortality, aligning with the goals of effective pest management.

From a biosafety standpoint, a genetically engineered pathogen should ideally not persist and reproduce prolifically in the field [72]. To alleviate environmental-safety concerns associated with genetically modified fungi, one primary approach is to reduce the ecological fitness or reproductive capability of the genetically engineered fungal strain [73–75]. In this study, the deficiency of MaCFEM1 mitigated the fungal colonization on the host cadaver. This potentially hampers the persistence and spread of the genetically engineered fungi, thereby mitigating concerns regarding genetic engineering.

In conclusion, this study revealed that following infection by an entomopathogenic fungus, certain predominant symbiotic bacteria within hosts exhibit potential pathogenicity. One of the factors determining their extensive proliferation in host hemocoel is the nutrients allocation dominated by the fungus. This study outlines a comprehensive network of interactions among hosts, symbiotic bacteria, and fungal pathogens. Building upon this theoretical framework, we highlight the synergistic role of the pathogenic fungus and symbiotic bacteria in promoting host mortality, thereby proposing a safe and effective strategy to enhance the efficacy of biopesticides in pest control.

Materials and methods

Locust rearing

The locusts (*Locusta migratoria*) were kept in the laboratory at the Institute of Zoology, Chinese Academy of

Sciences in Beijing. They were raised in well-ventilated cages measuring 50 × 50 × 50 cm, with approximately 200 locusts per cage. They were fed with fresh wheat seedlings. The culturing conditions were maintained at a constant temperature of 30 °C ± 2 °C, with a 14-h light and 10-h dark photo cycle. The experiments were conducted using fifth-instar nymphs.

Fungal and bacterial cultivation

The parental strain for generating deletions and overexpression strains was the *Metarhizium acridum* CQMa102 (GenBank: gb|ADNI00000000.1). Mature conidia were produced by culturing on one-quarter-strength Sabouraud dextrose (¼SDAY) agar for 15 days at 28 °C. The cloning experiments and protein expression were conducted using *E. coli* strains DH5 alpha and Origami-B (DE3) (WeiDi, EC1-2-M), respectively. The bacterial strains were grown in Luria–Bertani (LB) medium (Oxoid) at 37 °C. Fungal transformations were carried out using *Agrobacterium tumefaciens* AGL-1. The plasmid pET-22b (Qiyunbio, QP1140) was utilized for protein expression.

Quantification of fungal and bacterial loads in hemolymph of locusts

Aliquots (5 μL) of conidial suspension from the WT or Δ*MaCFEM1* strain were injected into the hemolymph of locusts at a concentration of 1×10^6 conidia/mL in 0.1% Tween-80 solution. For each strain, six groups of 10 locusts were used for each bioassay. The hemolymph was collected at different time points during the infection: 24, 48, 72, 96, and 120 hpi. For details, locusts were immersed in 75% ethanol for 3 min in order to completely eliminate the bacteria located on the epicuticle. Hemolymph was then collected at the base of the hind legs trough punching the arthrodial membrane. Mixed cells were harvested by centrifugation at 12,000 rpm for 2 min at 4 °C. Total RNA was extracted using the RNA Extraction Kit (CWBIO, CW0581S). The cDNA sample was synthesized using the Prime Script RT reagent kit (TakaRa, 6110A). *GPD* (Gene accession no. EFY84384) was used to determine the load of *M. aridum*. The bacterial load was quantified using the 16S-F/16S-R primers. qPCR analysis was conducted using the QuantStudio™ 1 Plus instrument (Thermo Fisher Scientific, A51693) and TB Green Master Mix (TakaRa, RR82WR). The ribosomal protein 49 (*rp49*) gene region of the locust was used as an internal reference. The relative RNA level of the *GPD* and 16 s rRNA gene was calculated using the $2^{-\Delta Ct}$ or $2^{-\Delta\Delta Ct}$ method. All primers used in this study are listed in Table S4.

Microbiome analysis

The inoculation of *M. acridum* was conducted as previously described. The collection of hemolymph and gut samples was conducted aseptically in a laminar hood. The control group was injected with sterile water only. The *M. acridum*-infected samples were collected at 96 hpi. Each sample was collected from 6 locusts, and 8 samples from each treatment were subjected to sequencing. All samples were flash-frozen in liquid nitrogen and ground using an automatic sample fast grinder JXFSTPRP-L (JingXin, JXFSTPRP-24L). Subsequent genomic DNA was isolated using the PowerFecal® Pro DNA Kits Isolation Kit (Qiagen, 51,804). The bacterial 16S rRNA gene of the V3-V4 region was PCR-amplified (ABI GeneAmp® 9700) using universal 16S rRNA gene-specific primers 338-F/806-R (Table S4). The quality of the DNA samples was checked on a 1.0% agarose gel. Paired ends (468 bp) were sequenced using the Illumina NovaSeq6000 platform by the service company Shanghai Majorbio Bio-Pharm Technology (Shanghai, China). High-quality Amplicon sequence variants (ASV) were derived and classified using DADA2. Taxonomic analysis and community diversity were conducted based on the valid data. Long-read sequencing of bacterial 16 s rRNA genes from the hemolymph sample was performed using the PacBio sequencing platform. The raw sequence data have been deposited in the Genome Sequence Archive in the National Genomics Data Center (https://ngdc.cncb.ac.cn/gsa). The assigned accession of the submission is CRA013449.

Antibiotic treatment

Axenic locusts were generated by injecting with triple antibiotic containing penicillin (50 mg/mL), streptomycin (30 mg/mL), and gentamicin (30 mg/mL) at 24 hpi with *M. acridum*. This procedure was repeated daily to maintain a continuous exposure of locusts to the antibiotics. Control locusts underwent the same method, but sterile water was used instead to ensure a comparable treatment.

Culturable bacterial isolate identification

Bacterial strains were obtained from locust hemolymph at 96 hpi with *M. acridum*. The hemolymph was diluted 10,000-fold with sterile water and 100 μL aliquots were spread onto LB and MRS agar plates (90 mm). The plates were then cultured at 37 °C for 48 h. Each treatment was performed in triplicate with 10 locusts per replicate. Single bacterial colonies were identified using PCR amplification with primers 27F and 1492R (Table S4). The resulting fragments were sequenced by

Tsingke (Beijing, China). The sequences were analyzed using BLAST to determine the bacterial species.

Fungal-bacterial cocultivation assays

Approximately 1×10^7 spores/mL (100 μL) fungal spores (WT and either Δ*MaCFEM1*, Δ*MaPR1C*, *ΔMaCWG* , and *ΔMaGLUS*) were grown in 30 mL ¼SDAY liquid medium at 28 ℃ while shaking at 200 rpm for 2 days. Then, the fungal cultures were inoculated with 1 mL of 0.5, 1.0, 3.0, 5.0, or 7.0 OD_{600}*E. faecalis* and *P. mirabilis* suspensions. The entire fungal mycelium was harvested after one day of co-culture using a suction pump. Final fungal biomass was weighed using a High Precise Electronic Balance (METTLER TOLEDO, MS2050DU). The bacterial CFU was determined by counting the number of bacterial plaques on the LB agar plate.

RNA sequencing and data processing

To test the gene expression profile of *M. acridum* in locusts, total RNA from the hemolymph of axenic and non-axenic locusts at 96 hpi with *M. acridum* was extracted using an RNA Extraction Kit (CWBIO, Beijing, China). Hyphal bodies and blastospores were harvested from hemolymph by centrifugation at 10,000 × g for 10 min at 4 °C. The supernatant was discarded, and the pellet containing hyphal bodies and blastospores was collected for RNA extraction. The cDNA libraries were prepared in accordance with the protocols of Illumina. A total of 12.5 Gbp filtered raw data were mapped to the genome of *Metarhizium acridum* CQMa102 strain (BioSample: SAMN02981259; GenBank: gb|ADNI00000000.1) via HISAT software. Among the reads aligned to the *M. acridum* genome, 80% mapped to exonic regions (Fig. S12A), with a coverage depth over 5 × (Table S5). The gene expression levels were measured using the criteria of Fragments Per Kilobase of exon model per Million (FPKM) mapped reads. Gene FPKM values across different samples exhibited similar distribution patterns (Fig. S12B and C). Saturation analysis indicated that as the number of sampled reads increased, the fluctuation of FPKM values for most genes (FPKM > 5, representing over 70% of the total genes) quickly stabilized (Fig. S12D and E). Therefore, the sequencing results accurately reflect gene expression levels. Differentially expressed genes (DEGs) were detected using the EdgeR software. The differences between the axenic and non-axenic groups were represented by adjusted *p* value. The DEGs with significance levels at adjusted *p* value < 0.05 in each comparison were considered as the candidate target genes.

For the in vitro co-culture assays, conidia of *Metarhizium acridum* were cultured in ¼ strength SDAY liquid medium for 24 h, either alone (control) or in co-culture with *Enterococcus faecalis*, *Proteus mirabilis*, *Staphylococcus aureus*, or *Escherichia coli,* respectively. The total RNA of *M. acridum* was extracted directly from *M. acridum* mycelium using a TRIzol reagent (Invitrogen). A total of 3 Gbp of filtered raw data were mapped to the genome of the *Metarhizium acridum* CQMa102 strain. The differences between the control and co-culture groups were represented by *p* value. The DEGs with significance levels at *p* value < 0.05 in each comparison were considered as the candidate target genes.

Gene quantification

The relative gene expression levels were quantified using the $2^{-\Delta Ct}$ or $2^{-\Delta\Delta Ct}$ method. For the quantification of fungal genes, *GPD* was used as the endogenous control. For the quantification of locust genes, *rp-49* was used as the endogenous control. At least five biological replicates were assayed for statistical analysis. The qPCR primers are listed in Table S4.

Generation of *M. acridum* mutant strains

DNA cassettes were generated using the homologous recombination technique to delete targeted genes. Approximately 1 kb of the 5′-flanking sequence and 3′-flanking sequence were amplified using primer pairs LF/LR and RF/RR from the template *M. acridum* Genomic DNA. These sequences were then cloned into the EcoRI/BamHI and XbaI/SacI restricted plasmid pDHt-Bar, respectively. The Bar resistance cassette, which confers resistance to bialaphos, was used as a selection marker for fungal transformation. The plasmids pDHt-Bar-MAC_04525, pDHt-Bar-MAC_07470, pDHt-Bar-MAC_05852, and pDHt-Bar-06277 were transformed into WT *M. acridum* strain, respectively, using *A. tumefaciens* mediated transformation. Transformants were screened on a Czapek-Dox medium containing 500 μg/mL Glufosinate ammonium (MedChemExpress, HY-W019870) and 250 μg/mL cefpirome (Mreda, M137862-5G). RT-PCR were used to verify the homologous integration of the resistance cassettes and the absence of genes. The primer pair gDNA-F/gDNA-R (Table S4) was used to verify the deletion of genomic DNA, while the primer pair V-F/V-R (Table S4) was used to verify the correct insertion of Bar in fungal genomes.

Virulence assays

For injection assays, conidiospores of the WT, Δ*MaCFEM1*, and *OE-MaCFEM1* strains were harvested from ¼SDAY agar plates and diluted to a final concentration of 1×10^6 conidiospores/mL in 0.1% Tween-80 solution. Five μL of the fungal suspensions were injected into fifth-instar locust nymphs. For topical infection assays, conidiospores were diluted to a final concentration of

1×10^8 conidiospores/mL. A 2.5 μL conidial suspension containing 1×10^8 conidia/mL was applied to the head-thorax junction of locusts. Locusts treated with 0.1% Tween-80 solution were used as the control. More than 30 locusts were used for each treatment. Insect mortality was recorded every 12 h. The experiments were repeated at least twice. The median lethal time (LT50) of each strain was calculated using Kaplan–Meier analysis, and the survival dynamics were compared using the log-rank test.

Bacterial single colonies were selected and grown overnight in LB at 37 °C while shaking at 200 rpm. The overnight cultures of *P. mirabilis*, *E. faecalis*, *E. hormaechei*, *K. aerogenes*, and *E. gallinarum* were resuspended to 10^8 CFU/mL in ultrapure water (Milli-Q). *W. confusa* was harvested from MRS medium and diluted in ultrapure water (Milli-Q) to a final concentration of 10^8 CFU/mL. Five μL of the bacterial suspensions was injected into fifth-instar nymphs of locusts. Control larvae were treated with ultrapure water (Milli-Q). Control and treated larvae were placed in an incubator and incubated at 30 °C. The number of dead insects was recorded every 12 h. The survival dynamics were compared by log-rank test.

Subcellular localization of MaCFEM1

The subcellular localization of MaCFEM1 was determined in the constitutive overexpression strain in which the MaCFEM1 was fused with a GFP gene. The GFP was inserted in MaCFEM1 between the signal peptide and the CFEM domain to achieve GFP-MaCFEM1 fusion. The *PgpdA* promoter from *Aspergillus Niger* was chosen and adapted for *M. acridum* to control the constitutive expression of *MaCFEM1*. Subcellular localization of GFP-MaCFEM1 was examined using Olympus SpinSR fluorescent microscopy (Olympus, Tokyo, Japan).

Recombinant protein expression and purification

To construct the recombinant plasmids of pET-22b-*MaCFEM*1-His, the *MaCFEM1* gene, without the signal peptide sequence, was amplified by using primers Eco-F/Eco-R (Table S4). Recombinant proteins of MaCFEM1 were expressed in the *E. coli* Origami B expression system. The recombinant plasmids were amplified in *E. coli* DH5α and were extracted using the TIANprep Mini Plasmid Kit (TIANGEN, DP103-02). Next, the recombinant plasmids were transformed into *E. coli* Origami B to generate a MaCFEM1-His fusion protein. Transformants were incubated at 37 °C with vigorous shaking for 6 h to $OD_{600}=0.6$, and then isopropyl β-d-1-thiogalactopyranoside (IPTG) (ThermoFisher, 15,529,019) in final concentration of 1 mM was added for induction at 18 °C with 200 rpm. The cultures were centrifuged for 30 min at 12,000 rpm, and washed with equilibration buffer (10 mM HEPES, 10 mM NaCl; pH 7.5). The cells were destroyed by an ultrasonic (SCIENTZ, 650E), and centrifuged at 13,000 rpm for 20 min. The supernatant was applied onto a nickel-nitrilotriacetic acid (Ni–NTA) affinity column (GE Healthcare, 17–5318-06) which was thoroughly washed with equilibration buffer to remove loosely bound protein with AKTA prime plus (GE Healthcare, 11,001,313). The recombinant protein was purified by a method linear-gradient elution method with different concentrations of imidazole. The purified protein was analyzed by SDS-PAGE.

Iron chelation resistance assay

To examine the iron chelation ability of MaCFEM1-His, titrations of purified protein into $Fe_2(SO4)_3$ were performed with a MicroCal iTC200 system (GE Healthcare, iTC200). MaCFEM1-His was concentrated to 5 mg/mL and buffer-exchanged into 1×PBS (pH 7.0) using a 10-kDa cutoff concentrator (Merck millipore, UFC801096). All solutions were prepared in 1×PBS buffer. $Fe_2(SO_4)_3$ (10 μM) solution was placed in the cell of the calorimeter and 100 mM MaCFEM1-His in 1×PBS buffer was loaded into the injection syringe. The recombinant protein was titrated into the cell at 25 °C as a sequence of 19 injections of 10 μL. All the injections were carried out at 120-s intervals. The sample cell was stirred throughout the experiment to ensure comprehensive mixing. The enthalpy (ΔH), stoichiometry of binding (N), and dissociation constants (K_D) were determined using the Origin for ITC software package. The titrations of MaCFEM1-His were conducted three times.

Antimicrobial effect of swainsonine

The antibacterial activity of swainsonine (MedChemExpress, HY-N6722) to *P. mirabilis* and *E. faecalis* was evaluated using the inhibition zone test. Swainsonine was dissolved in sterile water in a final concentration of 10 mM. *P. mirabilis* or *E. faecalis* (100 μL) at a concentration of $OD_{600}=0.01$/mL were spread evenly on LB plates. Swainsonine (100 μL) was added to an Oxford cup (OKLABS, njb5045) placed on the surface of the LB plates, and dual antibiotics containing ampicillin (50 μg/mL, 50 μL) and kanamycin (50 μg/mL, 50 μL) were added to the other Oxford cup as a positive control. The plates were incubated at 37 °C for 24 h.

Quantification of *iron* content in fungal mycelium and locust hemolymph

The concentrations of iron in the mycelium of both WT and the Δ*MaCFEM1*, as well as in locust hemolymph, were quantified using Inductively Coupled Plasma

Optical Emission Spectroscopy (ICP-OES) (ThermoFisher, Thermo ICPOES7200). For analysis, 0.1 g of fungal mycelium from the WT and Δ*MaCFEM1* was digested with 5 mL of concentrated nitric acid (69%). Additionally, 500 µL of cell-free hemolymph, pooled from at least twenty locusts, was processed with 5 mL of concentrated nitric acid. The samples' iron concentrations were subsequently measured by ICP-OES at the Beijing Zhongke Baice Technology Service Co., Ltd.

Iron depletion assays

The iron-depleted medium was created by incorporating the iron chelator ferrozine (FZ) (Coolaber, Beijing, China) into ¼SDAY agar or liquid medium at a final concentration of 1.0 mM. The fungal growth diameter was assessed by inoculating 1×10^6 spores/mL (2.5 µL) of WT or Δ*MaCFEM1* strains onto the iron-depleted plates for 6 days. The fungal colony sizes were determined using the ImageJ software (https://imagej.net/ij/). The expression levels of CFEM genes in *M. acridum* under iron-depleted conditions were examined by inoculating 1×10^7 spores/mL (100 µL) of *M. acridum* into 30 mL of iron-depleted liquid medium and incubating at 28 ℃ for 3 days. The mycelia of *M. acridum* were then harvested for RNA extraction.

Statistical analysis

For quantitative experiments, all data were statistically analyzed using GraphPad Prism 9.0 software and presented as mean ± SD. Student's *t*-test and Mann–Whitney *U* test were used for two-group comparison, one-way ANOVA followed by Bonfferroni's test, and Kruskal–Wallis test were used for multi-group comparisons. Survival data were analyzed using a Log-rank test. The normality of distribution was checked using the Shapiro–Wilk test. The equality of variances was analyzed using the F-test. Differences were considered as statistical significance at $p<0.05$. All samples were allocated into experimental groups randomly.

Supplementary Information

The online version contains supplementary material available at https://doi.org/10.1186/s40168-024-01928-4.

Additional file 1: Fig.S1 Quantification of bacterial and fungal loads in the hemolymph of locusts. A Growth of bacteria from hemolymph of noninfected locusts (control) and MAC-infected locusts at 96 h post injections (hpi). In the control group, a total volume of 40 µL hemolymph collected from 5 locusts in each treatment was plated onto LB agar plates. For the MAC-infected groups, hemolymph samples were diluted 104 times with sterile water before plating on LB plates. B Quantification of fungal load in the hemolymph of axenic and non-axenic locusts at 96 hpi with MAC ($n=6$, 5 locusts/replicate). Values are mean ± SD, significant differences are denoted by $^*p<0.05$, Mann–Whitney U test. C Expression of locust antimicrobial genes at 96 hpi with MAC ($n=6$, 5 locusts/replicate). One-way ANOVA with Bonfferroni's test for multiple comparisons. Values are mean ± s.e.m, significant differences are denoted by different letters. Fig.S2 Effects of the predominant symbiotic bacteria on MAC growth. Growth of MAC, E. faecalis, E. gallinarum, K. aerogenes, P. mirabilis and E. hormaechei colonies on LB agar plates, and growth of MAC and W. confusa on MRS agar plates. Fig.S3 The opportunistic bacteria are potential competitors of MAC in the locust. A Quantifications of E. faecalis and P. mirabilis loads in the hemocoel of locusts post bacterial injection ($n=6$, 3 locusts/replicate). B Absolute quantification of E. faecalis and P. mirabilis loads in the gut of locusts before (Control) and after MAC infection. Statistical differences were assessed using Student's t-test. Data are presented as mean ± s.e.m. Significance is denoted by $^{***}p<0.001$. C MAC mycelium biomass when co-cultured with different concentrations of bacterial isolates in ¼SDAY liquid medium. Differences between 0.0 OD600 and other concentrations were analyzed using One-way ANOVA with Bonferroni's test. Values are presented as mean ± SD, and significant differences are indicated by $^{**}p<0.01$, $^{***}p<0.001$. Fig. S4 Identification of genes encoding fungal lysozymes in MAC. A The phylogenetic tree illustrates the relationship among lysozyme orthologues in different Metarhizium species. The tree was constructed using the Neighbour-Joining method. B The protein structure of lysozymes in MAC. C Expression levels of MAC lysozyme-coding genes in vivo. Fig. S5 Induction of the swainsonine-biosynthetic cluster in the MAC by opportunistic bacteria. A The genome structure of swainsonine-biosynthetic cluster in MAC. B Expression pattern of the swainsonine-biosynthetic gene cluster in axenic and non-axenic locusts at 96 hpi with MAC. C Expression pattern of the swainsonine-biosynthetic gene cluster under co-culture conditions. B and C Heat map signals showing the log2 fold change values relative to the mean expression within each group. D The inhibition zone test revealing the lack of antimicrobial activity of swainsonine on E. faecalis and P. mirabilis. Fig. S6 The growth curves of E. faecalis, P. mirabilis, E. coli, and S. aureus in the 1/4 SDAY medium at 28 °C. Fig. S7 Verification of gene knockout efficiency. A PCR amplification of specific sequences of the target genes. B PCR amplification of combination for the outer sequence upstream of target gene and the inner sequence of biolaphos resistance (Bar) gene. Fig. S8 The structural analysis of MaCFEM1. A The three-dimensional structure of the CFEM domain of MaCFEM1 generated by the RoseTTAFold. B Sequence alignment of the CFEM domain of MaCFEM1 with that of Csa2, Pga7, and Rbt5. Csa2, Pga7, and Rbt5 are CFEM proteins known to participate in heme binding in Candida albicans. The regions in blue boxes represent the eight conserved cysteines, and the region in red box represents the aspartic acid residue with potential functions for iron-binding. Fig. S9 Systematic analysis of CFEM genes in MAC. A Identification and classification of CFEM genes in MAC. B Amino acid alignment of the CFEM domain of CFEM proteins in MAC. The regions in blue boxes represent the eight conserved cysteines, the regions in red boxes represent the aspartic acid residue with potential functions for iron binding. C Expression profiles of MAC CMEM genes in response to iron deficiency ($n=4$). Student's t-test for pairwise comparison. Values are mean ± SD, significant differences are denoted by $^*p<0.05$, $^{**}p<0.01$, and $^{***}p<0.001$, n.s represents no significant differences. D and E In vitro (D) and in vivo (E) expression profiles of the ten CFEM genes upon bacterial inductions. Heat map signals showing the log2 fold change values relative to the mean expression within each group. Fig. S10 Impact of MaCFEM1 deficiency on fungal hyphal body growth in locusts. Red arrows point to hyphal bodies, and the blue arrows point to locust hemocytes. Scale bar: 60 µm. The number of hyphal bodies are counted using hemocytometers ($n\geq7$, 3 locusts per replicates). Values are presented as mean ± s.e.m., differences between WT and ΔMaCFEM1-infected groups were analyzed using the Mann–Whitney U test, with significant differences denote as $^*p<0.05$. Fig. S11 Impact of iron deficiency on predominant symbiotic bacterial growth. To induce iron deficiency, the chelating agent Ferrozine (FZ) was supplemented to LB medium at a concentration of 5 mM. Colony sizes of the predominant symbiotic bacteria were quantified utilizing ImageJ software. Statistical differences between groups were evaluated using Student's t-test. Values are presented as mean ± SD. Significant differences are indicated by $^*p<0.05$. Scale bar: 2 cm. Fig. S12 Mapping rate analysis and gene expression maturation curve. A Proportion of reads mapped to exons, introns, and intergenic regions of the MAC genome. B Density distribution

plot of sequencing reads on MAC scaffolds. C Density distribution of gene expression levels for each sample. The x-axis represents the log2(FPKM) values, where higher values indicate higher gene expression levels. The y-axis represents the proportion of genes at each expression level relative to the total number of genes. D and E Gene saturation curves of axenic (D) and non-axenic (E) groups. Sequences were subsampled at 10%, 20%, …, up to 100%, and the gene expression levels obtained at different data amounts were compared with those obtained using all sequences. If the difference between the two values is less than 15%, the gene is considered to be accurately quantified at that data amount. For each gene, if the difference between the FPKM value estimated from the sample and the FPKM value using all reads is less than 15%, the expression level is considered accurately assessed. Table S1. Relative abundance of the top 12 bacterial taxa at the species level. Table S2. DEGs enriched in GO terms: Extracellular Region, External Encapsulating Structure, Cell Wall, Heme Binding, and Vitamin Binding. Table S3. DEGs potentially involve secondary metabolite synthesis and secretion. Table S4. Primers used in this study. Table S5. Mapping statistics

Acknowledgements
We thank HongRan Liu for her valuable contributions regarding the prediction of the MaCFEM1 protein structure.
Authors' contributions

Authors' contributions
L.K. conceived the project; D.D. and L.K. designed experiments; J.L., D.D., J.L., L.C., Q.C., and L.K. performed research; D.D., J.L., and L.K. analyzed data; and D.D., J.L., and L.K. wrote the paper.

Funding
This study was supported by the National Key Research and Development Program of China (Grant No. 2022YFD1400500); the National Science Foundation of China (Grant No. 32088102); Youth Innovation Promotion Association of Chinese Academy of Sciences (Grant No. 2023089); The State Key Laboratory of Integrated Management of Pest Insects and Rodents (Grant No. IPM2218).

Data availability
High throughput sequencing data of this study have been deposited in the National Genomics Data Center (https://ngdc.cncb.ac.cn/gsa). The raw data of bacterial 16 s rRNA gene sequencing are available at CRA012761 (https://ngdc.cncb.ac.cn/gsa/browse/CRA012761). The raw data of long-read sequencing of bacterial 16 s rRNA genes are available at CRA013449 (https://ngdc.cncb.ac.cn/gsa/browse/CRA013449). Fastq files of the transcriptome sequence are available at CRA012716 (https://ngdc.cncb.ac.cn/gsa/browse/CRA012716) and CRA012685 (https://ngdc.cncb.ac.cn/gsa/browse/CRA012685). All data are now publicly available.

Declarations

Ethics approval and consent to participate
Not applicable.

Consent for publication
Not applicable.

Competing interests
The authors declare that they have no competing interests.

Received: 16 April 2024 Accepted: 6 September 2024
Published online: 15 October 2024

References

1. Robinson CM. Enteric viruses exploit the microbiota to promote infection. Curr Opin Virol. 2019;37:58–62.
2. Jia D, Mao Q, Chen Y, Liu Y, Chen Q, Wu W, Zhang X, Chen H, Li Y, Wei T. Insect symbiotic bacteria harbour viral pathogens for transovarial transmission. Nat Microbiol. 2017;2:17025.
3. Kim EK, Lee KA, Hyeon DY, Kyung M, Jun KY, Seo SH, Hwang D, Kwon Y, Lee WJ. Bacterial nucleoside catabolism controls quorum sensing and commensal-to-pathogen transition in the gut. Cell Host Microbe. 2020;27(3):345–57.
4. Wei G, Lai Y, Wang G, Chen H, Li F, Wang S. Insect pathogenic fungus interacts with the gut microbiota to accelerate mosquito mortality. Proc Natl Acad Sci U S A. 2017;114(23):5994–9.
5. Narasimhan S, Rajeevan N, Liu L, Zhao YO, Heisig J, Pan JY, Eppler-Epstein R, DePonte K, Fish D, Fikrig E. Gut microbiota of the tick vector modulate colonization of the lyme disease spirochete. Cell Host Microbe. 2014;15(1):58–71.
6. Islam W, Adnan M, Shabbir A, Naveed H, Abubakar YS, Qasim M, Tayyab M, Noman A, Nisar MS, Khan KA, et al. Insect-fungal-interactions: a detailed review on entomopathogenic fungi pathogenicity to combat insect pests. Microb Pathog. 2021;159:105122.
7. Jiang YL, Wang JJ. The registration situation and use of mycopesticides in the world. J Fungi. 2023;9(9):940.
8. Sheng H, McNamara PJ, St Leger RJ. *Metarhizium*: an opportunistic middleman for multitrophic lifestyles. Curr Opin Microbiol. 2022;69:102176.
9. Wang C, St Leger RJ. A collagenous protective coat enables *Metarhizium anisopliae* to evade insect immune responses. Proc Natl Acad Sci U S A. 2006;103(17):6647–52.
10. Wang CS, Wang SB. Insect pathogenic fungi: genomics, molecular interactions, and genetic improvements. Annu Rev Entomol. 2017;62(62):73–90.
11. Shin TY, Lee MR, Park SE, Lee SJ, Kim WJ, Kim JS. Pathogenesis-related genes of entomopathogenic fungi. Arch Insect Biochem. 2020;105(4): e21747.
12. Shang J, Hong S, Wang C. Fights on the surface prior to fungal invasion of insects. PLoS Pathog. 2024;20(2):e1011994.
13. Toledo AV, Alippi AM, Lenicov AMMD. Growth inhibition of *Beauveria bassiana* by bacteria isolated from the cuticular surface of the corn leafhopper, *Dalbulus maidis* and the planthopper, *Delphacodes kuscheli*, two important vectors of maize pathogens. J Insect Sci. 2011;11:1–13.
14. Pessotti RD, Hansen BL, Reaso JN, Ceja-Navarro JA, El-Hifnawi L, Brodie EL, Traxler MF. Multiple lineages of streptomyces produce antimicrobials within passalid beetle galleries across eastern North America. Elife. 2021;10:e65091.
15. Dillon RJ, Charnley AK. Invasion of the pathogenic fungus *Metarhizium Anisopliae* through the guts of germ-free desert locusts. Schistocerca Gregaria. Mycopathologia. 1986;96(1):59–66.
16. Dillon RJ, Vennard CT, Buckling A, Charnley AK. Diversity of locust gut bacteria protects against pathogen invasion. Ecol Lett. 2005;8(12):1291–8.
17. Arango RA, Carlson CM, Currie CR, McDonald BR, Book AJ, Green F 3rd, Lebow NK, Raffa KF. Antimicrobial activity of actinobacteria isolated from the guts of subterranean termites. Environ Entomol. 2016;45(6):1415–23.
18. Miller DL, Smith EA, Newton ILG. A bacterial symbiont protects honey bees from fungal disease. mBio. 2021;12(3):e0050321.
19. Bai J, Xu Z, Li L, Zhang Y, Diao J, Cao J, Xu L, Ma L. Gut bacterial microbiota of *Lymantria dispar asiatica* and its involvement in *Beauveria bassiana* infection. J Invertebr Pathol. 2023;197:107897.
20. Wang Z, Cheng Y, Wang Y, Yu X. Topical fungal infection induces shifts in the gut microbiota structure of brown planthopper, *Nilaparvata lugens* (Homoptera: Delphacidae). Insects. 2022;13(6):528.
21. Wang JL, Sun J, Song YJ, Zheng HH, Wang GJ, Luo WX, Li L, Liu XS. An entomopathogenic fungus exploits its host humoral antibacterial immunity to minimize bacterial competition in the hemolymph. Microbiome. 2023;11(1):116.
22. Sun YL, Hong S, Chen HM, Yin Y, Wang CS. Production of helvolic acid in *Metarhizium* contributes to fungal infection of insects by bacteriostatic inhibition of the host cuticular microbiomes. Microbiol Spectr. 2022;10(5):e0262022.
23. Hong S, Sun Y, Chen H, Wang C. Suppression of the insect cuticular microbiomes by a fungal defensin to facilitate parasite infection. ISME J. 2023;17(1):1–11.
24. Lovett B, Bilgo E, Diabate A, St Leger R. A review of progress toward field application of transgenic mosquitocidal entomopathogenic fungi. Pest Manag Sci. 2019;75(9):2316–24.

25. Wang C, St Leger RJ. A scorpion neurotoxin increases the potency of a fungal insecticide. Nat Biotechnol. 2007;25(12):1455–6.
26. Lovett B, Bilgo E, Millogo SA, Ouattarra AK, Sare I, Gnambani EJ, Dabire RK, Diabate A, St Leger RJ. Transgenic *Metarhizium* rapidly kills mosquitoes in a malaria-endemic region of Burkina Faso. Science. 2019;364(6443):894–7.
27. Wang Y, Cui C, Wang G, Li Y, Wang S. Insects defend against fungal infection by employing microRNAs to silence virulence-related genes. Proc Natl Acad Sci U S A. 2021;118(19):e2023802118.
28. Ding D, Zhang J, Du BZ, Wang XZ, Hou L, Guo SY, Chen B, Kang L. Non-canonical function of an Hif-1 alpha splice variant contributes to the sustained flight of locusts. Elife. 2022;11:e74554.
29. Du BZ, Ding D, Ma C, Guo W, Kang L. Locust density shapes energy metabolism and oxidative stress resulting in divergence of flight traits. P Natl Acad Sci USA. 2022;119(1):e2115753118.
30. Guo XJ, Yu QQ, Chen DF, Wei JN, Yang PC, Yu J, Wang XH, Kang L. 4-Vinylanisole is an aggregation pheromone in locusts. Nature. 2020;584(7822):584–8.
31. Zhang L, Lecoq M, Latchininsky A, Hunter D. Locust and grasshopper management. Annu Rev Entomol. 2019;64:15–34.
32. Prior C, Carey M, Abraham YJ, Moore D, Bateman RP. Development of a bioassay method for the selection of entomopathogenic fungi virulent to the desert locust, *Schistocerca Gregaria* (Forskal). J Appl Entomol. 1995;119(8):567–73.
33. Driver F, Milner RJ, Trueman JWH. A taxonomic revision of *Metarhizium* based on a phylogenetic analysis of rDNA sequence data. Mycol Res. 2000;104:134–50.
34. Tong X, Wang Y, Yang P, Wang C, Kang L. Tryptamine accumulation caused by deletion of MrMao-1 in *Metarhizium* genome significantly enhances insecticidal virulence. PLoS Genet. 2020;16(4):e1008675.
35. Gao QA, Jin K, Ying SH, Zhang YJ, Xiao GH, Shang YF, Duan ZB, Hu XA, Xie XQ, Zhou G, et al. Genome sequencing and comparative transcriptomics of the model entomopathogenic fungi Metarhizium anisopliae and M. acridum. Plos Genetics. 2011;7(1):e1001264.
36. Hu X, Xiao G, Zheng P, Shang Y, Su Y, Zhang X, Liu X, Zhan S, St Leger RJ, Wang C. Trajectory and genomic determinants of fungal-pathogen speciation and host adaptation. Proc Natl Acad Sci U S A. 2014;111(47):16796–801.
37. Boomsma JJ, Jensen AB, Meyling NV, Eilenberg J. Evolutionary interaction networks of insect pathogenic fungi. Annu Rev Entomol. 2014;59:467–85.
38. Sim KL, Perry D. Swainsonine production by *Metarhizium Anisopliae* determined by means of an enzymatic assay. Mycol Res. 1995;99:1078–82.
39. Cook D, Gardner DR, Pfister JA. Swainsonine-containing plants and their relationship to endophytic fungi. J Agr Food Chem. 2014;62(30):7326–34.
40. Baek M, DiMaio F, Anishchenko I, Dauparas J, Ovchinnikov S, Lee GR, Wang J, Cong Q, Kinch LN, Schaeffer RD, et al. Accurate prediction of protein structures and interactions using a three-track neural network. Science. 2021;373(6557):871–6.
41. Nasser L, Weissman Z, Pinsky M, Amartely H, Dvir H, Kornitzer D. Structural basis of haem-iron acquisition by fungal pathogens. Nat Microbiol. 2016;1(11):16156.
42. Kuznets G, Vigonsky E, Weissman Z, Lalli D, Gildor T, Kauffman SJ, Turano P, Becker J, Lewinson O, Kornitzer D. A relay network of extracellular heme-binding proteins drives C. albicans iron acquisition from hemoglobin. PLoS Pathog. 2014;10(10):e1004407.
43. Wang F, Xin CY, Liu JX, Ran ZN, Zhao CL, Song ZY. Interactions between invasive fungi and symbiotic bacteria. World J Microb Biot. 2020;36(9):137.
44. Lu MT, Wei DX, Shang JM, Li SQ, Song SX, Luo YJ, Tang GR, Wang CS. Suppression of antifungal immunity by a parasite effector via blocking GNBP3 and GNBP-like 3, the dual receptors for b-glucans. Cell Rep. 2024;43(1):113642.
45. Wang JJ, Hu HW, Pang SY, Yin XY, Cao BH, Huang JL, Xu XL, Weng QF, Hu QB. Destruxin A inhibits the hemocytin-mediated hemolymph immunity of host insects to facilitate infection. Cell Rep. 2024;43(2):113686.
46. Stevens EJ, Bates KA, King KC. Host microbiota can facilitate pathogen infection. PLoS Pathog. 2021;17(5):e1009514.
47. Broderick NA, Raffa KF, Handelsman J. Midgut bacteria required for *Bacillus thuringiensis* insecticidal activity. P Natl Acad Sci USA. 2006;103(41):15196–9.
48. Mason KL, Stepien TA, Blum JE, Holt JF, Labbe NH, Rush JS, Raffa KF, Handelsman J. From commensal to pathogen: translocation of Enterococcus faecalis from the midgut to the hemocoel of Manduca sexta. mBio. 2011;2(3):e00065-00011.
49. Caccia S, Di Lelio I, La Storia A, Marinelli A, Varricchio P, Franzetti E, Banyuls N, Tettamanti G, Casartelli M, Giordana B, et al. Midgut microbiota and host immunocompetence underlie *Bacillus thuringiensis* killing mechanism. Proc Natl Acad Sci U S A. 2016;113(34):9486–91.
50. Ma Q, Fonseca A, Liu WQ, Fields AT, Pimsler ML, Spindola AF, Tarone AM, Crippen TL, Tomberlin JK, Wood TK. Proteus mirabilis interkingdom swarming signals attract blow flies. ISME J. 2012;6(7):1356–66.
51. Martin JD, Mundt JO. Enterococci in insects. Appl Microbiol. 1972;24(4):575-+.
52. Kryukov VY, Kosman E, Tomilova O, Polenogova O, Rotskaya U, Tyurin M, Alikina T, Yaroslavtseva O, Kabilov M, Glupov V. Interplay between fungal infection and bacterial associates in the wax moth *Galleria mellonella* under different temperature conditions. J Fungi (Basel). 2020;6(3):170.
53. Broll V, Perin APA, Lopes FC, Martinelli AHS, Moyetta NR, Fruttero LL, Grahl MVC, Uberti AF, Demartini DR, Ligabue-Braun R, et al. Non-enzymatic properties of Proteus mirabilis urease subunits. Process Biochem. 2021;110:263–74.
54. Lieu PT, Heiskala M, Peterson PA, Yang Y. The roles of iron in health and disease. Mol Aspects Med. 2001;22(1–2):1–87.
55. Emerit J, Beaumont C, Trivin F. Iron metabolism, free radicals, and oxidative injury. Biomed Pharmacother. 2001;55(6):333–9.
56. Hentze MW, Muckenthaler MU, Galy B, Camaschella C. Two to tango: regulation of mammalian iron metabolism. Cell. 2010;142(1):24–38.
57. Gorman MJ. Iron homeostasis in insects. Annu Rev Entomol. 2023;68:51–67.
58. Hood MI, Skaar EP. Nutritional immunity: transition metals at the pathogen-host interface. Nat Rev Microbiol. 2012;10(8):525–37.
59. Iatsenko I, Marra A, Boquete JP, Pena J, Lemaitre B. Iron sequestration by transferrin 1 mediates nutritional immunity in *Drosophila melanogaster*. Proc Natl Acad Sci U S A. 2020;117(13):7317–25.
60. Kulkarni RD, Kelkar HS, Dean RA. An eight-cysteine-containing CFEM domain unique to a group of fungal membrane proteins. Trends Biochem Sci. 2003;28(3):118–21.
61. Zhang ZN, Wu QY, Zhang GZ, Zhu YY, Murphy RW, Liu Z, Zou CG. Systematic analyses reveal uniqueness and origin of the CFEM domain in fungi. Sci Rep. 2015;5:13032.
62. Zuo N, Bai WZ, Wei WQ, Yuan TL, Zhang D, Wang YZ, Tang WH. Fungal CFEM effectors negatively regulate a maize wall-associated kinase by interacting with its alternatively spliced variant to dampen resistance. Cell Rep. 2022;41(13):111877.
63. Sabnam N, Roy Barman S. WISH, a novel CFEM GPCR is indispensable for surface sensing, asexual and pathogenic differentiation in rice blast fungus. Fungal Genet Biol. 2017;105:37–51.
64. Kou YJ, Tan YH, Ramanujam R, Naqvi NI. Structure-function analyses of the Pth11 receptor reveal an important role for CFEM motif and redox regulation in rice blast. New Phytol. 2017;214(1):330–42.
65. Shang J, Tang G, Yang J, Lu M, Wang CZ, Wang C. Sensing of a spore surface protein by a *Drosophila* chemosensory protein induces behavioral defense against fungal parasitic infections. Curr Biol. 2023;33(2):276–86.
66. Roy U, Yaish S, Weissman Z, Pinsky M, Dey S, Horev G, Kornitzer D. Ferric reductase-related proteins mediate fungal heme acquisition. Elife. 2022;11:e80604.
67. Peng YJ, Hou J, Zhang H, Lei JH, Lin HY, Ding JL, Feng MG, Ying SH. Systematic contributions of CFEM domain-containing proteins to iron acquisition are essential for interspecies interaction of the filamentous pathogenic fungus *Beauveria bassiana*. Environ Microbiol. 2022;24(8):3693–704.
68. Wang D, Zhang DD, Song J, Li JJ, Wang J, Li R, Klosterman SJ, Kong ZQ, Lin FZ, Dai XF, et al. *Verticillium dahliae* CFEM proteins manipulate host immunity and differentially contribute to virulence. BMC Biol. 2022;20(1):55.
69. Srivastava VK, Suneetha KJ, Kaur R. A systematic analysis reveals an essential role for high-affinity iron uptake system, haemolysin and CFEM domain-containing protein in iron homoeostasis and virulence in *Candida glabrata*. Biochem J. 2014;463(1):103–14.
70. Giuliano Garisto Donzelli B, Gibson DM, Krasnoff SB. Intracellular siderophore but not extracellular siderophore is required for full virulence in Metarhizium robertsii. Fungal Genet Biol. 2015;82:56–68.
71. St Leger RJ, Wang JB. *Metarhizium*: jack of all trades, master of many. Open Biol. 2020;10(12):200307.

72. Zhao H, Lovett B, Fang W. Genetically engineering entomopathogenic fungi. Adv Genet. 2016;94:137–63.
73. St Leger R, Joshi L, Bidochka MJ, Roberts DW. Construction of an improved mycoinsecticide overexpressing a toxic protease. Proc Natl Acad Sci U S A. 1996;93(13):6349–54.
74. Liu YJ, Liu J, Ying SH, Liu SS, Feng MG. A fungal insecticide engineered for fast killing of caterpillars has high field efficacy and safety in full-season control of cabbage insect pests. Appl Environ Microb. 2013;79(20):6452–8.
75. Lu D, Pava-Ripoll M, Li Z, Wang C. Insecticidal evaluation of *Beauveria bassiana* engineered to express a scorpion neurotoxin and a cuticle degrading protease. Appl Microbiol Biotechnol. 2008;81(3):515–22.

Publisher's Note